Journal of Biomedical Engineering and Medical Imaging

TABLE OF CONTENTS

DISCLAIMER

Wavelet-based Image Fusion for Enhancement of ROI in CT Image

Nguyen Thanh Hai
Faculty of Electrical-Electronic Engineering, UTE-HCMC, Vietnam;
nthai@hcmute.edu.vn

ABSTRACT

This paper proposes a novel method for enhancing Computed Tomography (CT) image. In this proposed method, the entropy-based histogram algorithm was applied to detach significant values in CT image to produce a detached image. In addition, wavelet transforms were employed for both the original CT image and the detached image to create image fusion. Therefore, an enhanced image with tumor region was obtained for diagnosis using an inverse wavelet transform. The result is that the processed region in the enhanced image shows more prominent points than that in the original image. This result can allow physicians or doctors diagnose and predict more accurately tumor regions in the enhanced CT image.

Keywords: CT image, Wavelet Transform, Image Enhancement, Fusion Image.

1. INTRODUCTION

Cancer is a century disease which can occur in anyone's body. The most importance of cancer problem is to diagnose and detect it earlier for treatment. In practice, there are a few technologies of medical imaging such as Positron Emission Tomography (PET), Magnetic Resonance imaging (MRI), Computed Tomography (CT) and Ultrasound [1-3]. However, image processing is always applied for improving medical images. This allows doctors more easily diagnose and predict cancer diseases.

In biomedical image processing, different approaches have been proposed for detection of Regions of Interest (ROI) [4]. In lung image, segmentation algorithm was applied to enhance local anatomical structure using geometric and intensity models. In particular, morphology-based ROI segmentation was combined with watershed transform for comparative analysis in noisy environment [5]. A. Kumar, et al. developed a graph-based Content-based image retrieval (CBIR) method to exploit 3D spatial features extracted from volumetric ROIs [6]. In addition,

authors applied a graph edit distance for measurement of the similarity of PET-CT images based on the spatial arrangement of tumors and organs.

Wavelet transform [7] has been applied for image processing to filter or to find features. An efficient algorithm for removing noise from corrupted images incorporating a wavelet-based threshold with a spatial based joint bilateral filter [8]. In this method, the performances for image denoising on a number of standard images were evaluated based on signal to noise ratio. Another application is that the author et al. applied wavelet transform with Haar function for image denoising [9]. The result is that image noise was effectively reduced and improved through the evaluation of the peak signal-to-noise ratio.

For Enhancement of medical image, a proposed method of pre-restoration adjustment phase was applied [10]. To low contrast images, an adaptive histogram equalization was employed with six stages. Moreover, authors tested this algorithm with over fifty medical images and also compared the processed image results with previous works. Finally, the conducted results with various features to illustrate the effectiveness of the proposed method. Another research is that a wavelet transform was employed for enhancement of CT image [11]. Authors tested the proposed method to 118 patients with cancers and 60 with benign tumors in this study. The results indicated that the image enhancement using the proposed method improved the diagnosis accuracy.

In this paper, for image enhancement to be better quality than an original CT image, histogram and entropy values of the image are processed and computed. Thus, in the proposed method, the remarkable region in the original image detached and then transformed using a wavelet transform with Harr function. In addition, the wavelet transform are employed to compute the original image to produce a wavelet image. A combined algorithm is applied to produce image fusion. An enhanced image is created after an inverse wavelet transform.

2. METHOD

In general, an original CT image with tumor region will be enhanced for diagnosis. Firstly, the original CT image is transformed to produce a histogram image. Based on this histogram image, one can calculate entropy statistics to obtain an image with significant values, called the detach image. This detach image and the original image are transformed to create image fusion using decomposition wavelet transforms. For diagnosis, the inverse wavelet transform is utilized to obtain an enhanced image as shown in Figure 1.
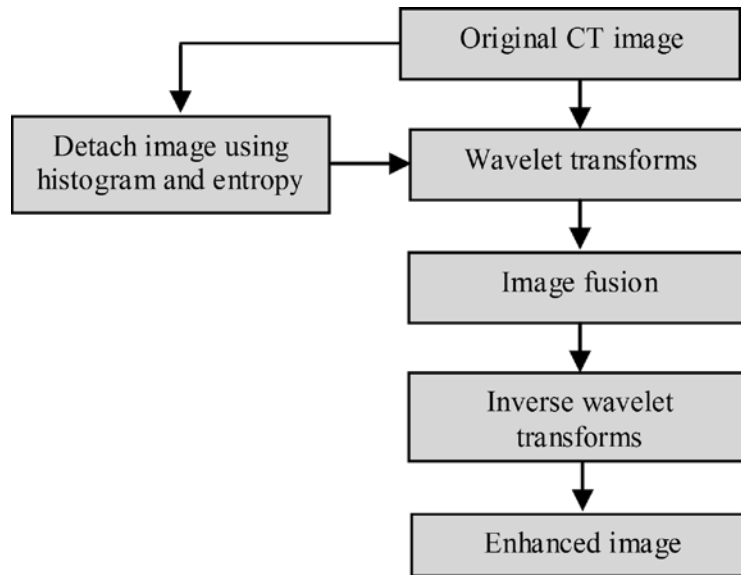
Figure 1: Block diagram of computing an enhancement image

The proposed method will be applied to process an original image of a patient with the circled region, in which there is Region of Interest (ROI), called the interrogative region to tumors, as shown in Figure 2. This region represents many details, in which there are some points addressed by arrows for enhancement.
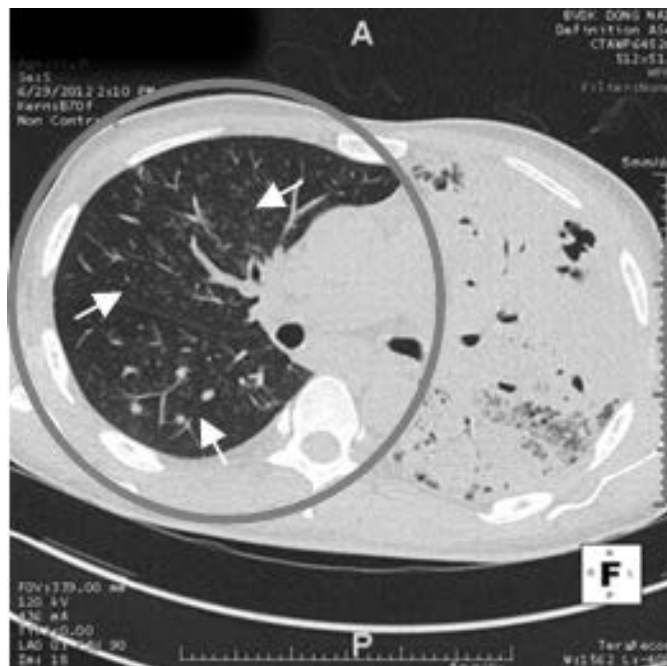
Figure 2: CT image of a patient (provided by Dong Nai hospital, Vietnam)

2.1 Detach of Image using Histogram and Entropy

For enhancement of image using information of histogram and entropy, one needs to determine a histogram map. Consider an CT image *f(m,n)* with the MxN size, in which gray levels *l=0,1,2,…,255*. The histogram of the image is defined as follows:

$$hist_{f(m,n)}(l) = \sum_{m=0}^{M-1}\sum_{n=0}^{N-1} \delta_d(f(m,n)-l) \tag{1}$$

where the discrete unit impulse function is expressed as the following function:

$$\delta_d(k) = \begin{cases} 1 & k=0 \\ 0 & otherwise \end{cases} \tag{2}$$

In order to determine gray levels in an image, a histogram map is calculated as shown in Figure 3a using Eq. (1). The histogram may be normalized by dividing its entries by the total number of pixels in the image for image fusion. The normalized histogram, which may be taken to represent the probability density function $p_f(l)$ for generating the fused image, is expressed as follows:

$$p_f(l) = \frac{1}{\sum_{l=0}^{255} hist_{f(m,n)}(l)} * hist_{f(m,n)}(l) \tag{3}$$

where $p_f(l)$ denotes the normalized histogram, *f(m,n)* represents the gray levels of the image,

l=0,1,2,…,255 and $\sum_{l=0}^{255} p_f(l) = 1$.

Figure 3: Representation of histogram images, (a) histogram of the original CT image with 256 gray-levels and pixels; (b) histogram after normalizing with 256 gray-levels and levels in [0 1].

Figure 3 shows two histogram maps with gray levels vs. pixel density, in which Figure 4a is the histogram of the original image and Figure 3b represents the histogram of the normalized image with the gray levels in [0 1] for determination of image information.
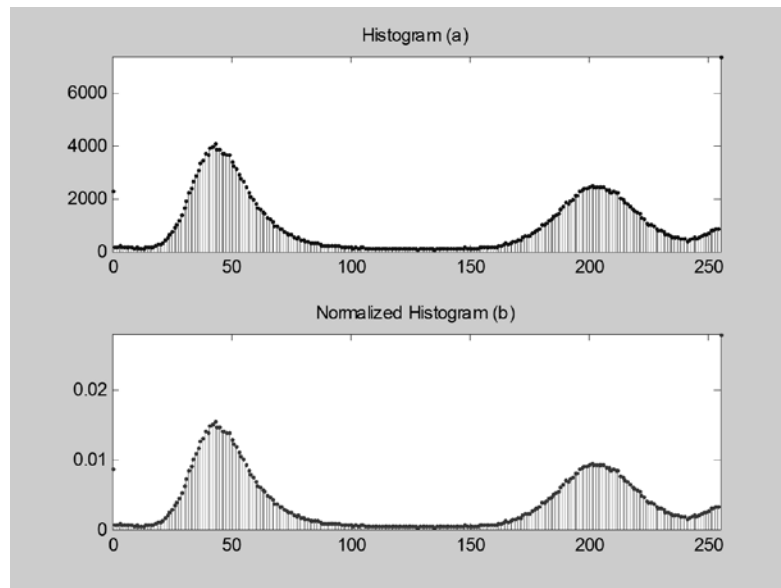
For calculation of image information $h(p_l)$, $l=0,1,2,...,255$, one can measure conveyable information corresponding to each different gray level in the 2D image. This relates to the probability of gray levels in an image. Indeed, a totally unexpected event conveys maximal information when it occurs, where $p_f(l) = 0$ for $h(p_l) = \infty$ and an event, that is certain to occur, does not convey any information, where $p_f(l) = 1$ for $h(p_l) = 0$. Then if the more $h(p_l)$ is small, the more gray-level will carry important transmitter information in image. Therefore, the set of the information values $h(p_l)$ can be determined using the following expression:

$$h(p_l) = -\log\big(p_f(l)\big)$$

(4)

Based on the probability of gray levels, its entropy *H* is calculated for determining pixels with the highest information. The equation to calculate the entropy values is described as follows:

$$H = -\sum_{l=0}^{255} p_f(l) * \log_2\big(p_f(l)\big)$$

(5)

From information of the normalized histogram map and the entropy, one can determine values with the highest information of the image. Based on these information, the neighborhood pixels around these pixel values can be split to produce a detached image.

In particular, based on the normalized histogram, the gray values of the lowest probability can be determined. For example, assume that the gray level is 128 and the value of information $h(p_l)$=0.004 for l = 128, it can be recognized that this is the important value in image and it should be detached for image enhancement. However, the problem is that how many points in the detached image is reasonable. In this case, one can use a coefficient, called *Δcof*. If the selection of the coefficient Δcof is appropriate, the processed image has good quality. Assume that $h(p_l)$=0.004 is chosen, it is very hard to distinguish the processed image and the original image due to differences between two entropies such as $H_{\Delta cof}$=7.2695 (the processed image) and H_0=7.2696 (the original image). In this case, its error must be less than 2% (Weber's Law states that the ratio of the increment threshold to the background intensity is a constant). Therefore, we need to adjust this error by selecting the coefficient Δcof to obtain a desired value for creating the high quality information in the image. Thereby, one can detach many important values in the image and the value of the information h_o to be extracted is defined as follows:

$$h_o = \min\big(h(p_l)\big) + \Delta cof$$

(6)

where $\Delta cof = 0.001$, $h_o = 0.005$ is obtained. Therefore, we need to detach the information to be $h_{p(l)} \leq h_o$. From these values, a set of $Q(q)$ is obtained, where q is the set of quantity $h_{p(l)}$, is satisfied the above conditions.

Table 1: Parameters of entropy information in image with Δcof

Δcof	ho	Q(q)	h_{pl}(min)	h_{pl}(max)	$H_{\Delta cof}$
0.000	0.004	1	128	128	7.2695
0.001	0.005	11	115	142	7.2555
0.002	0.006	45	107	149	7.1763
0.003	0.007	62	101	155	7.1386
0.004	0.008	76	96	161	7.0985
0.005	0.009	86	11	161	7.0772
0.020	0.024	147	3	250	6.7145
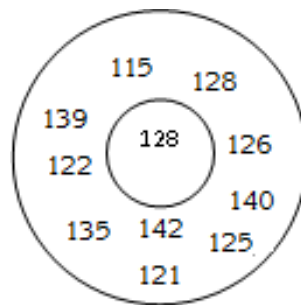
Figure 4: Neighborhood region the gray-level-value l= 128 which convey the highest information

When *Q(q)* includes **11** different gray-level values, that are *115, 121, 122, 125, 126, 128, 135, 139, 140* and *142*. These gray-level values are nearby with gray-level value *l=128* and *h(pl)=0.005* that is presented in Figure 4. From these points, one will detach them from an original image in order to get a proposed detached image.

Table 2 shows a few cases with many different coefficients Δcof selected for comparison and evaluation. When the coefficient Δcof is selected increasingly, the values of information *h(pl)* will increase. This means that the information of gray levels in the image are declined due to many sets of quantity in *Q(q)* have no necessary information. Figures 5a and 5b represent detached images corresponding to different coefficients Δcof and the object edges in Figure 5b are better that in Figure 5a.

(a)   (b)
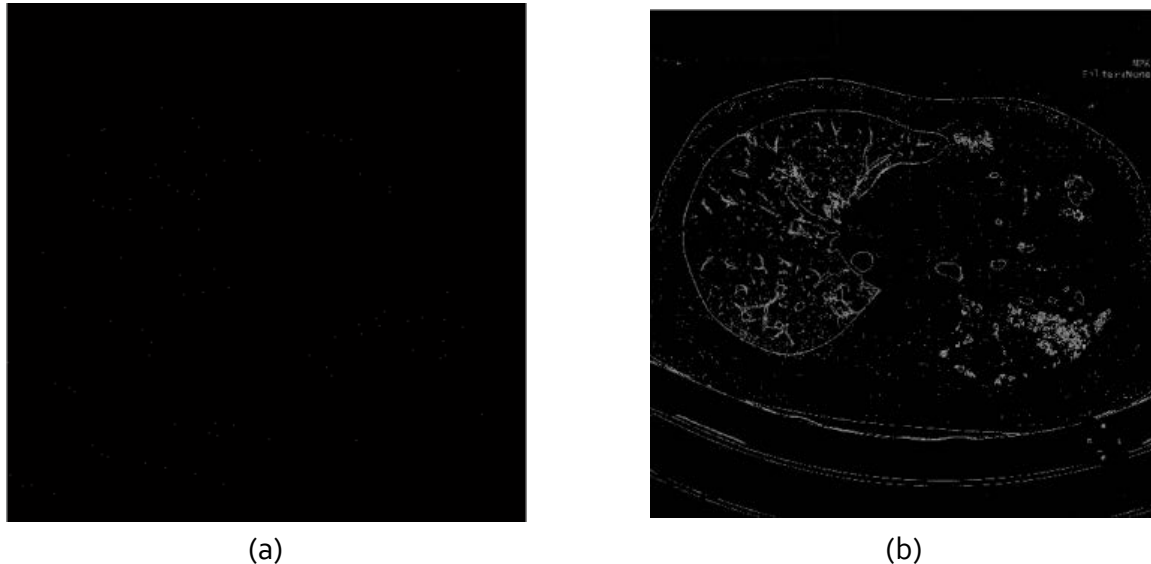
Figure 5: Detach image with different coefficients: (a) Δcof **=0.000; (b)** Δcof **=0.005**

From the histogram algorithm, the novel detach image algorithm, which is built, can detach each gray-level of the image to create the set of different gray-levels from 0 to 255. Assume that *G* is the set of 256 pixel values from 256 gray-levels in CT image and is expressed as follows:

$$G = \sum_{m=0}^{M-1}\sum_{n=0}^{N-1} g_l(m,n) = (\delta_d(f(m,n)-l))*l \qquad (7)$$

where *l=0,1,2,…,255* respectively and δ_d is the discrete unit impulse function). From Eq. (7) we will get 256 arrays, every array includes one gray-level value and its position in image from 0 to 255. Assume that detach image based on Δcof *fd(m,n)* can be calculated by combining between the G matrix of gray levels and the values *Q(q)* using the following formulas:

$$g_L(m,n) = g_l(m,n)*(\delta_d(l-Q(q))) \qquad (8)$$

$$f_d(m,n) = \sum_{i=0}^{255} g_l(m,n) \qquad (9)$$

where *l=0:255* and *q=1:length[Q(q)]*.

2.2 Wavelet transforms with Harr function

For image enhancement, wavelet transform with Harr function are utilized for both the detached image and the original image to produce wavelet images. Therefore, one detaches these two wavelet images to create image fusion. The purpose of Haar-type Wavelet Transforms (HWT) is to filter noise around the suspected areas. A CT image *f(m,n)* can be considered as a matrix of the *M x N* image, in which columns A denotes a^1,a^2,…,a^N. The HWT applied for each column of A is C, which is defined as follows:

$$C = W_N A = \left(W_N \, \mathbf{a}^1, W_N \, \mathbf{a}^2, ..., W_N \, \mathbf{a}^N \right) \tag{10}$$

Therefore, the rows of *C* are continuously processed and then multiply the second side of Eq. (11) and the matrix W_M^T, one has:

$$CW_M^T = W_N A W_M^T$$

Thus, the 2D HWT of the *M x N* matrix A is represented as follows:

$$B = W_N A W_M^T \tag{11}$$

where $B = CW_M^T$. Assume that CT image is *f(m,n)* and considered as a matrix of the 512x512 image. Thus, we can define $W_{512} = [H \,|\, G]$ and transform it to obtain as follows:

$$W_{512} A W_{512}^T = \begin{bmatrix} H \\ G \end{bmatrix} A \begin{bmatrix} H^T \,|\, G^T \end{bmatrix} = \begin{bmatrix} HAH^T & HAG^T \\ GAH^T & GAG^T \end{bmatrix} \tag{12}$$

where H and G are the 256x512 matrices.

$$H = \begin{bmatrix} \frac{1}{2} & \frac{1}{2} & 0 & 0 & ... & ... & 0 & 0 \\ 0 & 0 & \frac{1}{2} & \frac{1}{2} & ... & ... & 0 & 0 \\ ... & ... & ... & ... & ... & ... & ... & ... \\ 0 & 0 & 0 & 0 & ... & ... & \frac{1}{2} & \frac{1}{2} \end{bmatrix} \tag{13}$$

$$G = \begin{bmatrix} -\frac{1}{2} & -\frac{1}{2} & 0 & 0 & ... & ... & 0 & 0 \\ 0 & 0 & -\frac{1}{2} & -\frac{1}{2} & ... & ... & 0 & 0 \\ ... & ... & ... & ... & ... & ... & ... & ... \\ 0 & 0 & 0 & 0 & ... & ... & -\frac{1}{2} & -\frac{1}{2} \end{bmatrix} \tag{14}$$

From Eq. (14), one divided image into four parts of HWT image (called *B, V, H and D*). In particular, HAH^T (B) is an approximation of the original image; GAG^T (H) can be viewed as differences along the rows of the image; similarly HAG^T (V) are differences along the columns of image and the fourth part is that GAG^T (D) are described as differences along the diagonal of image. The objective of this method is to release the area *D* due to it is the noisy area in this image.

Using two levels of the Wavelet transforms in Eq. (12) with coefficients *H,G* in Eq. (13) and Eq. (14) for the original image *f(m,n)* and the detached image *f$_d$(m,n)*. The result is that *f$_w$(m,n)* and *f$_{wd}$(m,n)* are obtained as shown in Fig. 6 and Fig.7.
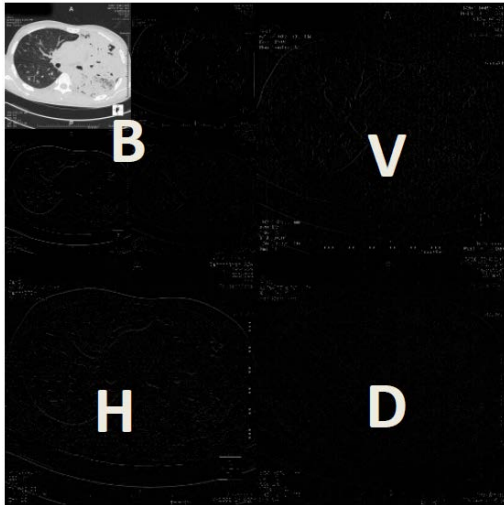
Figure 6: Original image with two HWT levels
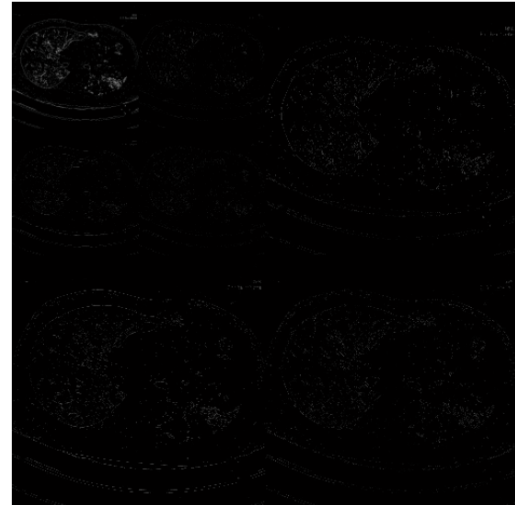
Figure 7: detached image with two HWT levels

2.3   Image fusion

In this paper, the wavelet transform method was applied to combine images to produce the fused image. The fusion process is that the input images are decomposed into the multi-scale edge representation using the HWT in the different wavelet domains. In addition, the fused multi-scale representation is built based on pixel-by-pixel to produce the fused image and it is computed using the following expression:

$$f_{fusion}(m,n) = \begin{cases} f_w(m,n) + f_{wd}(m,n) & f_w(m,n) + f_{wd}(m,n) < 255 \\ 255 & f_w(m,n) + f_{wd}(m,n) \geq 255 \end{cases} \tag{15}$$

The advantage of this algorithm is easily performed. However, it would be difficult to observe them and the loss of gray-level values in image can occur if the gray-level values have identical positions. That will impact to other neighboring regions in image. But, we just concern with the marked locations, so it is temporarily ignored and the obtained image still give an effective image.

2.4   Inverse wavelet transform algorithm

In order to reconstruct the original image with enhancement for more easily observation, the inverse wavelet transforms is employed. From Eq. (11) and Eq. (12), an enhancement image is described using the following equation:

$$f_{final}(m,n) = \left(W_{512}\right)' f_{fusion}(m,n) \left(W_{512}^{T}\right)' \tag{16}$$

where W' is the inverse matrix transform and W^T is the transposition matrix.

3. RESULTS AND DISCUSSION

From the original CT image as shown in Fig. 8, the iterative procedure is performed in this method to process several lung cancer CT images with the different coefficients Δcof. Moreover, this method, which depends on the entropy value of gray-levels in the image, is

employed around the area which appears small details with blur related to the tumor problem. The result is that the enhanced images are represented corresponding to the coefficients Δcof as shown in Figures 9 - 11. Each image with a different coefficient will give an enhanced image and it depends on doctors' choice for diagnosis.
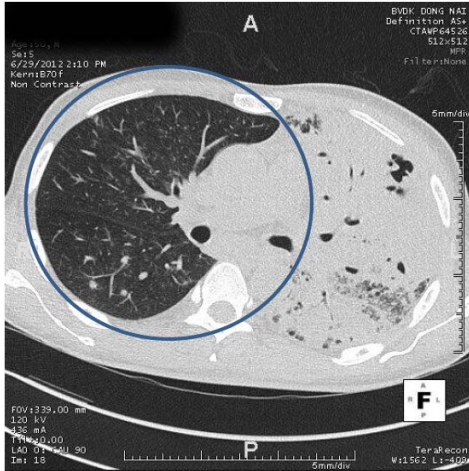
Figure 8: Original CT image of patient predicted lung cancer
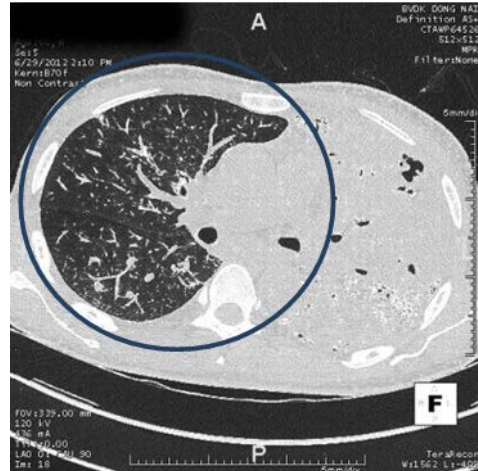
Figure 10: Enhanced image with coefficient Δcof=0.005
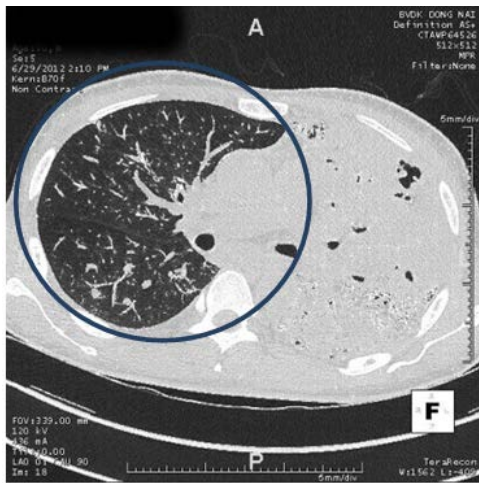
Figure 9: Enhanced CT image with coefficient Δcof=0.003

Figure 11: Enhanced CT image with coefficient Δcof=0.009

In comparison between Figure 9, Figure 10 and Figure 10, the initial requirement is that the ROI with the enhanced details has been found to be sharper and clearer. Moreover, details of vascular, pulmonary capillaries in the lung have been clarified. Additions to other areas, the outside of the circle, which do not need to consider due to the objective of the paper just aims to process remarkable regions in CT image. Since the process of biopsy, diagnosis will be followed by a team of researchers and doctors to make decision of the most accurate diagnosis for patients. In this research, the coefficient Δcof plays an important role due to it decides the

detached image with the set of gray level quantity *Q(q)* related to the quality level of enhancement image.

(a)

(b)

(c)

(d)

(e)

(f)
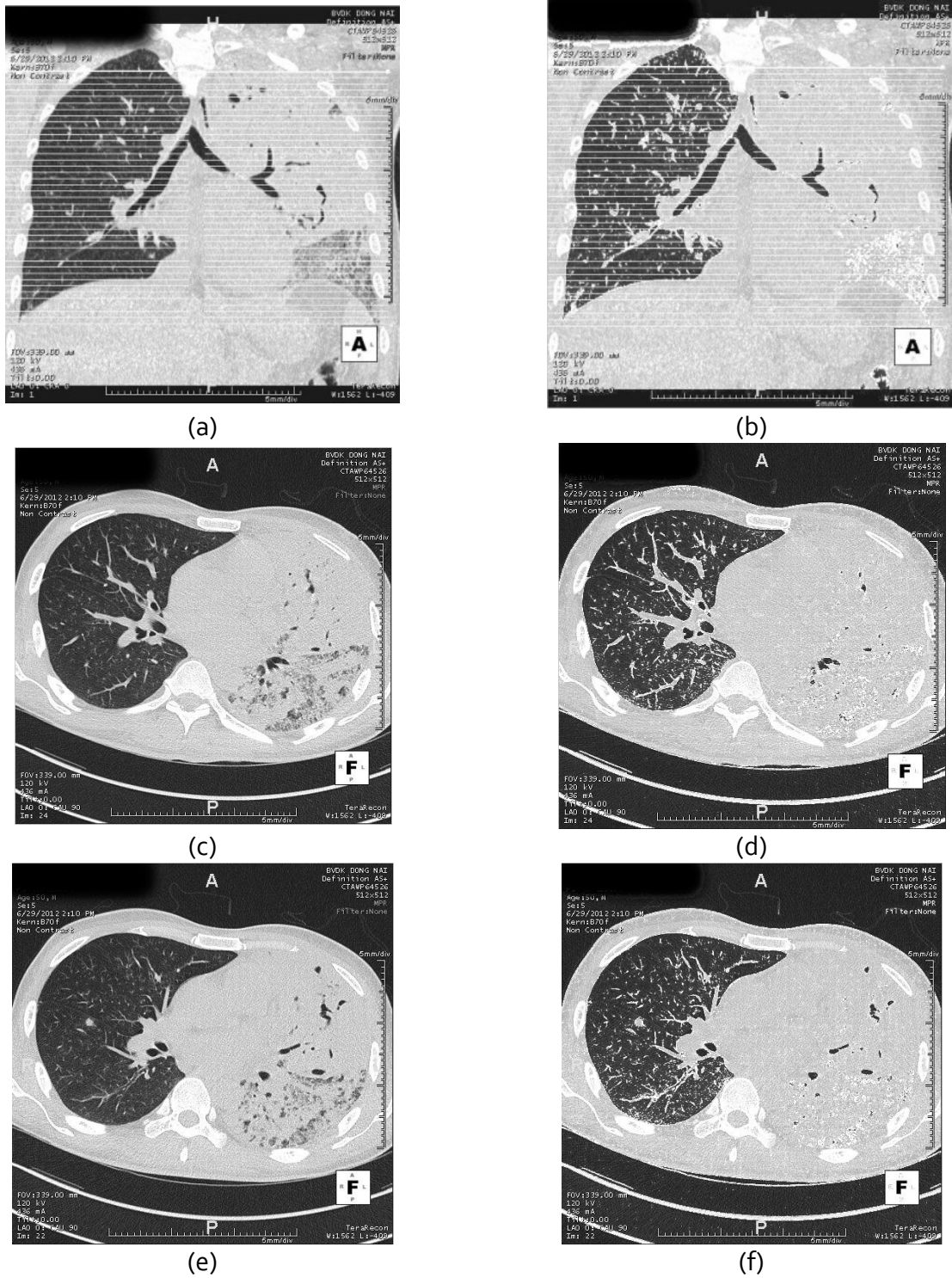
Figure 12: (a),(c) and (e) are the original CT images of a patient predicted lung cancer;

(b),(d) and (f) are the CT images processed with coefficient Δ*cof* = 0.007

In order to increasingly evaluate the proposed method, more different results are shown in Figure 12, in which Figures (a), (c) and (e) are original images and Figures (b), (d) and (f) are images after processing with the coefficient Δcof=0.007.

On the issue of relating to enhancement image, how to select the optimal coefficients Δcof and the most accuracy is very important. One found that the (>0.02) ratio is too high or (>0.005) is too, the image points, which are too bright, glitzy, high contrast, are so many unnecessary during image processing or they do not affect the enhanced image. Because these image points can be the lack of necessary information when the low coefficient values Δcof are chosen.

4. Conclusion

This paper showed an image fusion novel method based on the Wavelet Transform with Harr function (HWT). In particular, the detached image developed from a histogram entropy approach was matched with an original image through the HWT to produce image fusion. In this image fusion method, several techniques were used such as optical expression, contrast coefficient, histogram, entropy, gray-scale transforms and gray-scale windows to create an enhanced image. The enhanced image showed brilliant points and regions of interest (ROIs) with good quality compared with the original image. Simulation results showed to illustrate the effectiveness of the proposed method.

ACKNOWLEDGMENT

REFERENCES

[1].   J. E. Mackewn, G. Charles-Edwards, and J.J. Totman, P. Halsted, E.J. Somer, S.F. Keevil, P.K. Marsden "A fiducial marker based technique for alignment of simultaneously acquired PET and MRI images," in *Nuclear Science Symposium Conference Record* 2009.

[2].   E. A. Hoffman, J. M. Reinhardt, and M. Sonka, "Characterization of the interstitial lung diseases via density-based and texture-based analysis of computed tomography images of lung structure and function," *Academic Radiology,* vol. 10, pp. 1104–1118, 2003.

[3].   L. J. Brattain, C. Floryan, O. P. Hauser, and M. Nguyen, "Simple and effective ultrasound needle guidance system," in *The Annual International Conference of the IEEE on Engineering in Medicine and Biology Society*, 2011.

[4]. J. Huang, F. Jian, H. Wu, and H. Li, "An improved level set method for vertebra CT image segmentation," *BioMedical Engineering OnLine,* 2013.

[5]. V.V Kishore and R.V.S. Satyanarayana, "Performance evaluation of edge detectors - morphology based ROI segmentation and nodule detection from DICOM lung images in the noisy environment," in *The 2013 IEEE 3rd international conference on Advance Computing Conference*, 2013.

[6]. A. Kumar, J. Kim, L. Wen, D. Feng, "A Graph-based approach to the retrieval of volumetric PET-CT lung images," in *The 2012 Annual International Conference of the IEEE on Engineering in Medicine and Biology Society (EMBC)*, 2012.

[7]. HaozhengRen, YihuaLan, and Y. Zhang, "Research of multi-focus image fusion based on M-band multi-wavelet transformation," in *The 2011 Fourth International Workshop on Advanced Computational Intelligence*, 2011.

[8]. V.C. Bibina, V. S., and S. Viswasom,"Adaptive wavelet thresholding and joint bilateral filtering for image denoising," in *The 2012 Annual IEEE India Conference (INDICON)*, 2012.

[9]. Y. Qiang, "Image denoisingbased on Haar wavelet transform," in *The 2011 International Conference on Electronics and Optoelectronics (ICEOE)*, 2011.

[10]. Zohair Al-Ameen, Ghazali Sulong, Md. Gapar Md. Johar, "Employing a Suitable Contrast Enhancement Technique as a pre-restoration adjustment phase for Computed Tomography Medical Image", International Journal of Bio-Science and Bio-Technology, Vol. 5, No. 1, Feb, 2013.

[11]. Xiuhua G., Xiangye L., Huan W., Zhigang L., Wei W., Qian H., Kuncheng L., Wei W., "Enhanced CT Image by the Wavelet Transform Improving Diagnostic Accuracy of Chest Nodules", Journal of Digital Imaging, Vol. 24, No. 1, 2011.

Abnormality Detection in Ovarian Ultrasound Images using Active Contours

Usha B S[1], Sandya S[2]

[1]*Research Scholar (ECE, VTU), RNS Institute of Technology, Bengaluru, India*
2*Nitte Meenakshi Institute of Technology, Bengaluru, India*
bsusha@gmail.com, sandya9prasad@gmail.com

ABSTRACT

Analyzing ovarian size parameters and its shape is the first hand information required in Ovary diagnosis. Automated segmentation of Ovary and measuring its size and analyzing its shape can help doctors in mass screening programme in faster diagnosis. In this paper, we propose a new improved algorithm (anisotropic diffusion filter, CLAHE enhancement, and active contour segmentation) to extract the Ovary from its homogeneous background followed by geometrical and shape feature extraction of the Ovary for automated computer-assisted analysis. The proposed algorithm is tested on 75 Transvaginal ultrasound images of ovaries. The experimental results are validated against the manual measurements done by the expert and the results obtained by our algorithm are in good agreement with experts inputs. The proposed algorithm could achieve an average Error Percentage EM_1 of 4% for Major-Axis length and average Error Percentage EM_2 of 5.43% for Minor-Axis length and classification rate of 91.66%.

Keywords: Image segmentation, Ovary, anisotropic diffusion filter, active contour, Geometric features, Ovary classification

1. INTRODUCTION

Ultrasound imaging has become an integral diagnostic tool to evaluate the gynecological health of a woman [1]. In this paper, we propose a new modified algorithm for computer-assisted analysis of the ultrasound images of women's ovaries. Ovary is scanned to diagnose abnormalities like infertility, irregular menstrual cycles, PCOS, cysts, tumors etc. Analyzing the ovarian size parameters and its shape are one of the first steps in diagnosis of the Ovary [1-3].The normal range of Ovary size parameters is listed in Table I which was obtained in literature and supported by our expert Dr. Sriprada Vinekar, Gynecologist and Sonographist. Lists the parameters considered to evaluate the shape of the Ovary. Values listed in Table 1 are used to evaluate whether Ovary is normal or abnormal.

Table 1: Ovary Condition

Normal Ovary	Min	Max
Major-axis length M1	3cm	5cm
Minor-axis length M2	1.5cm	3cm
Thickness	0.5cm	1.5cm
Area	$3.54cm^2$	$11.8cm^2$
Perimeter	7.45cm	12.95cm
Form Factor F	0.8	0.88
Compactness Q	14.2	15.6
Eccentricity E	>0.5	
Shape	Oval (Almond)	

2. BACKGROUND WORK

Automated measurement of ovarian parameters requires segmentation of the Ovary from the ovarian ultrasound images. The ultrasound images are of low contrast and poor quality due to the presence of speckle noise. Moreover the Region of Interest (Ovary) is highly homogeneous with its background. Hence, edge preserving speckle filters are required to improve the image quality and possibly the diagnostic potential of the image. In [1] Bilateral filter proposed by Tomasi C, Manduchi R[4] was used for speckle removal, Contrast Stretching and Power Law Transformation were used for enhancement, adaptive Thresholding and Global Thresholding for segmentation to extract Ovary. The average Error Percentage for Major-Axis length (E_{M1}) obtained was 11.9% and the average Error Percentage for Minor-Axis length (E_{M2}) obtained was 17.4%. In [2] anisotropic diffusion filter proposed by Perona and Malik [5, 6] was used for speckle reduction, CLAHE [7] followed by adaptive binary thresholding to extract Ovary. The algorithm could achieve an average Error Percentage of 5.27% for Major-Axis length (E_{M1}) and average Error Percentage of 6.1% for Minor-Axis length (E_{M2}). In [8, 9] active contours was used for detection of follicles. The average detection rate was 96.66%, false rejection rate (FRR) 3.33 %, and false acceptance rate (FAR) 15.04%. Active contours detect edges even in high noisy region and hence in this paper we propose to use active contours for segmentation.

The paper is organized as follows: Section III provides the description of the algorithm where speckle reduction filter, contrast enhancement methods, segmentation techniques and feature extraction are explained in detail. Section IV, the experimental results are discussed along with manual measurements done by the expert and section V contains conclusions and future scope of work.

3. MEASUREMENT OF OVARIAN FEATURES AND CLASSIFICATION

The input is a Transvaginal ultrasound image of Ovary acquired from GE-LOGIQ Book XP ultrasound machine which is a high performance multipurpose color hand-carried imaging system. The images are obtained in JPEG-LS (24-bit, 532x434x3) format. The sample ultrasound image is shown in Figure.1 consists of the Ovary region and Ovarian follicles inside the Ovary.
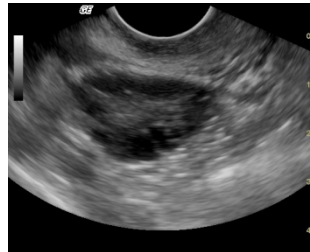
Figure. 1   Ultrasound Ovary image

The input image has identical RGB planes hence, only R-plane (8-bit, 532x434) is considered as the input image. The position of the Region of Interest, Ovary in all images is in the center of the fan area, so a sub-image I_{ROI} containing only the Ovary (ROI) of size [310 420] is extracted.

3.1   Preprocessing

The proposed Ovary feature extraction system is shown in Figure.2. Measurement of the size and shape features of the Ovary requires segmentation of the Ovary from the ultrasound image. Since ultrasound images are invariably noisy due to speckle noise, we use speckle reducing anisotropic diffusion filter for denoising. The edge magnitude parameter k was chosen as 0.9 and number of iterations fixed at 5. The filtered output I_{f2} has very good mean preservation, variance reduction, and edge localization.
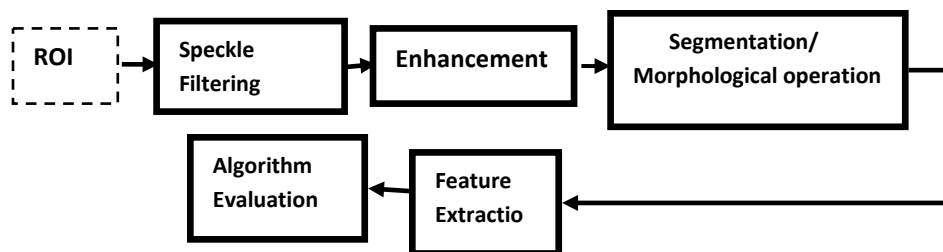
Figure.2 Ovary Feature Extraction System

To create a good contrast between the Ovary and the background which is essential for segmentation, Contrast Limited Adaptive Histogram Equalization (CLAHE) is applied. This algorithm operates on small data regions (tiles), instead of an entire image. Each tile's contrast is enhanced using Rayleigh's distribution. The neighboring tiles are combined using bilinear interpolation to eliminate artificially induced boundaries. In this algorithm we have chosen the tile value as [3 2], each tile's contrast is enhanced using Rayleigh's distribution. The clip-limit is

chosen as 0.1, range as original and alpha which is a distribution parameter is chosen as 6. The output of the enhancement stage ICL(x,y) has a clear contrast between Ovary and background and is suitable for segmentation.

3.2   Processing

The processing stage has Segmentation, Morphological operation and feature extraction. The active contours without edges are used for segmentation. The resulting image after segmentation has many regions apart from Ovary. To begin with regions touching the image border are removed followed by region filling operation. We next perform morphological erosion (3 times with window size 3x3) followed by morphological dilation (3 times with window size 3x3). Many small phantom regions exist along with the Ovary region. A connected component labeling algorithm finds all connected components in the image and assigns a unique label to all points in the same component. Regions having smaller area than the threshold T are removed. This might result with more than one component. The Centroid (C= Cx, Cy) of the remaining components are found. In the current database, the Ovary is in the middle of the fan area and the mean centroid (C= Cx, Cy) of Ovary is experimentally found. Rule1 & Rule2 shown below are used to retain Ovary and eliminate the rest of the regions/components.

Rule1: $\mu Cx - k\ \sigma Cx\ \ \le\ \ Cx \le \mu Cx + k\sigma Cx$

Rule2: $\mu Cy - k\ \sigma Cy\ \ \le\ \ Cy \le \mu Cy + k\sigma Cy$

3.3   Feature Extraction

The outcome of the processing stage is a single component, Ovary. The sample input Ovary and the segmentation result is shown in Figure.3.
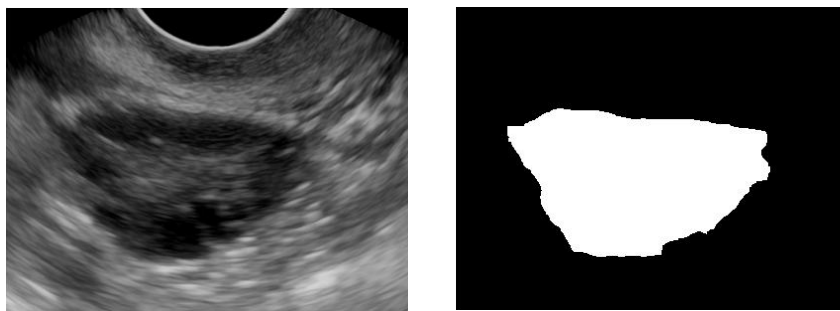
Figure.3 Segmentation result of Ovary

The geometrical and shape features of the segmented region are extracted which are grouped under F1 and F2 feature sets. The feature set F1: is the size based features and F2: is the shape based features [3].

F1: This feature set includes the Major-axis length M1, Minor-axis length M2, Area A and Perimeter P.

F2: This feature set includes Form Factor F, Compactness Q, and Eccentricity E.

3.4   Classification

In the training phase, the F1 and F2 feature sets of the ovaries are extracted. The mean and standard deviation of each of this parameter is calculated. The µ and σ of these parameters are listed in TABLE 2. Based on these values classification rules are formulated as shown in TABLE 3.

Table 2: mean and Standard deviations

Parameter	Mean, sigma
$\mu M_1, \sigma M_1$	3.459, 0.757
$\mu M_2, \sigma M_2$	1.987, 0.565
$\mu A, \sigma A$	5.494, 2.5936
$\mu P, \sigma P$	10.28, 2.82
$\mu F, \sigma_F$	0.8451,0.12
$\mu Q, \sigma_Q$	15.15, 2.97
$\mu C_x, \sigma_{Cx}$	191.32, 37.65
$\mu C_y, \sigma_{Cy}$	110.77, 27.277

The classification rules of the kσ-Classifier are formulated as in TABLE IV. A region is classified as a normal Ovary, if the following conditions Rulei, i=1,2,…..9 are satisfied. The value of constant k is 2, α is 0.3 in the experiment. All the values are empirically determined.

Table 3: Rules

Rule1: $\mu Cx - k\, \sigma Cx \ \leq \ Cx \leq \mu Cx + k\sigma Cx$

Rule2: $\mu Cy - k\, \sigma Cy \ \leq \ Cy \leq \mu Cy + k\sigma Cy$

Rule3: $\mu M_1 - k/3\, \sigma M_1 + \alpha \leq M_1 \leq \mu M_1 + k\sigma M_1 + \alpha$

Rule4: $\mu M_2 - k/3\, \sigma M_2 + \alpha \leq M2 \leq \mu M_2 + k\sigma M_2 + \alpha$

Rule5: $\mu A - k/2\, \sigma A + \alpha \leq A \leq \mu A + k\, \sigma A + 2\, \alpha$

Rule6: $\mu P - k/2\, \sigma P + \alpha \leq P \leq \mu P + k\, \sigma P + \alpha$

Rule7: $\mu F - k\, \sigma_F \ \leq F \leq \mu F + k\, \sigma_F$

Rule8: $\mu Q - k\, \sigma_Q \ \leq \ Q \leq \mu Q + k\, \sigma_Q$

Rule9: $\mu E - k\, \sigma_E \ \leq \ E \leq \mu E + k\, \sigma_E$

In the testing phase, Feature set F1 and F2 are computed for the segmented region of Ovary and the classification rules Rulei are applied to determine whether the Ovary is normal or not. Rule1 & Rule2 1 are applied to retain Ovary and eliminate other regions when multiple regions of same size are the segmentation outcome. Rule3 to Rule6 classifies the Ovary based on size and are the key rules for classifying. R8 to R9 are based on shape and support the Rule3-6.

3.5   Performance Measures

The accuracy of Ovary segmentation is measured using two parameters- the error percentage [1, 2] for Major-axis length (EM1) and Minor-axis length (EM2) which is used to evaluate and validate the algorithm. We calculate the percentage error between the expert measured value of M1 and M2 and algorithm evaluated value of M1 and M2. This parameter qualifies the algorithm as to how best or how near the algorithm is to the expert measured values. It is required that ideally the error percentage is "ZERO" but a ±12% deviation is acceptable as per the expert.

The error percentage [1, 2] for Major-axis length (EM1) and Minor-axis length (EM2) is calculated by using (1) and (2).

$$E_{M1} = \frac{|((length)_{obtained\ value} - (length)_{Expert\ value})|}{(length)_{Expert\ value}} X\ 100 \tag{1}$$

$$E_{M2} = \frac{|((width)_{obtained\ value} - (width)_{Expert\ value})|}{(width)_{Expert\ value}} X\ 100 \tag{2}$$

Ovary segmentation process, might result in more than one regions. So in order to select the Ovary we use Rule 1 & 2. But if there are more than one regions with in the centroid with allowable variance, algorithm might select a wrong region as Ovary. This might lead to misclassification. An Ovary is classified either as normal or abnormal. Consequently, there are four events; two classifications and two misclassifications.

3.5.1 Classification Rate

The classification rate or classification accuracy is estimated by the ratio of the total number of correctly classified Ovary images (sum of true positives and true negatives) by the number of input Ovary images.

$$Classification\ Rate = \frac{\#of\ Correctly\ Classified\ Ovary\ Images}{\#of\ Input\ Ovary\ Images} \tag{3}$$

3.5.2 False Acceptance Rate

False acceptance, also called a type II error, is defined as the percentage of abnormal Ovary images classified as normal.

3.5.3 False Rejection Rate

False Rejection Ratio, also called a type I error, is defined as the percentage of normal Ovary images misclassified as abnormal.

4. RESULTS AND DISCUSSIONS

The database consists of 75 Transvaginal ultrasound images of ovaries. The size parameter M1 and M2 are provided by the expert for all the 75 images. The classification output is validated against the expert inputs. In our experiment, 40 images are used in training phase and 35 (20 normal, 15 abnormal) in testing phase. The sample outputs where the edge of the segmented Ovary is superimposed on the input image for subjective validation by the expert are shown in Fig 4. The first column of images shows the expert measured values of Major-axis length M1 and Minor axis length M2 and the second column shows the output images. The F1 features and F2 features and classification output of the sample images are shown in Table VI. The average Error Percentage obtained is 4% for Major-Axis length (EM1) and 5.45% for Minor-Axis length (EM2) which is very much lesser than the BCAT method or ACAT method [3]. EM1 was 11.9% and EM2 was 17.4% using BCAT method whereas EM1 was 5.27% and EM2 was 6.1% using ACAT method. The average Error percentage using our new algorithm is very insignificant and proves to be better than ACAT and BCAT method.

The K-σ classifier rules listed in TABLE IV is applied to the feature set F1, F2 to classify the Ovary as normal or abnormal. Out of 35 images used for testing, 20 images are normal and 15 images are abnormal. Classification results obtained by the algorithm is discussed below:

Among 20 normal Ovary images 18 are classified as normal and 2 are classified as abnormal. Among 15 abnormal images, 14 are classified as abnormal and 1 image is classified as normal. The classification rate is 91.66% and false acceptance rate (FAR) is 6.66% and false rejection rate (FRR) is 10% respectively.

The classification rate has significantly improved to 91.66% with our new algorithm compared to BCAT method in which classification rate was 76.67% and ACAT method in which classification rate was 85.8%. The TABLE 4 shows the classification results.

Table 4: Resuts

Methodology	Classification Rate	Type II Error (FAR)	Type I Error(FRR)
New Algorithm	91.66%	6.66%	10%
BCAT	76.67%	26.66%	20%
ACAT	85.8%	13.33%	15%

5. CONCLUSIONS

The classification rate depends on the choice of filter used, enhancement methods and segmentation method. The average Error Percentage is 4% for EM1 and 5.45% for EM2 which is significantly better than BCAT and ACAT method. From TABLE 5 it can be inferred that ACA has a good classification rate of 91.66%, FAR of 6.66% and FRR of 10%. The algorithm can be further improved using filters that can preserve edges better and segmentation methods that can extract the Ovary.
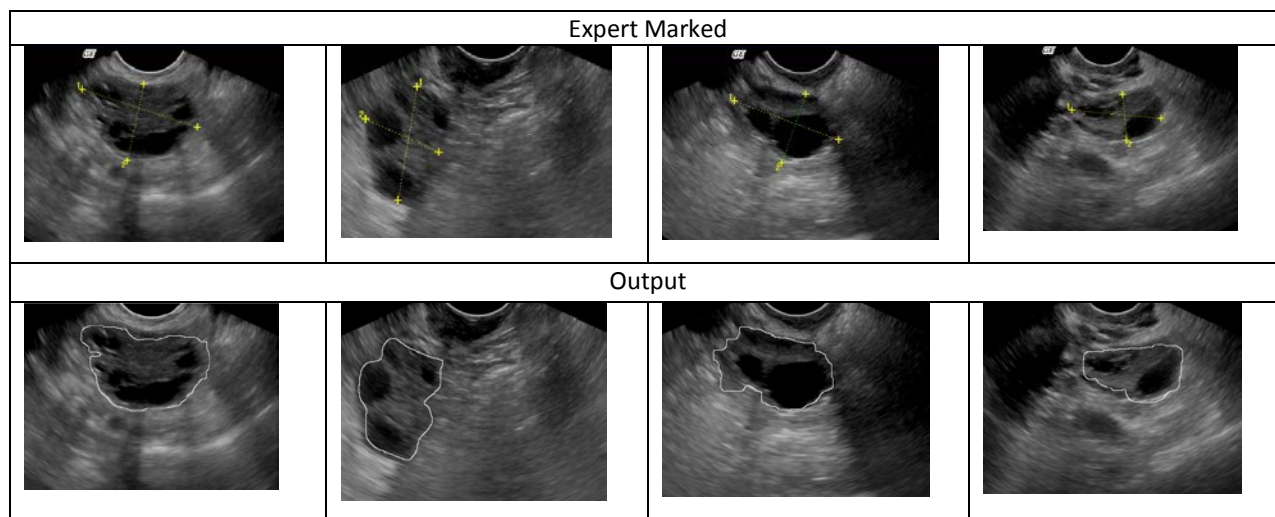
Figure 4. Segmentation results

Table 5: Classification Rates

#	M_1(Expert)	M_2(Expert)	M_1(Cm)	M_2(Cm)	A(Cm^2)	P(Cm)	F	Q	E	Classification
1	2.84	1.41	2.838	1.443	3.14	6.75	0.86	14.51	0.86	Normal
2	4.08	1.14	4.220	1.33	3.65	9.82	0.45	16.52	0.949	Normal
3	3.04	1.7	3.073	1.749	4.19	7.83	0.85	14.6	0.8221	Normal
4	3.04	1.7	2.936	1.645	3.77	7.45	0.85	14.72	0.8283	Normal
5	2.81	2.1	2.771	2.030	4.41	7.62	0.95	13.16	0.6806	Normal
6	4.14	1.17	4.202	1.134	3.72	9.66	0.5	25	0.9692	Normal
7	4.1	3.32	4.0155	3.2479	10.17	11.45	0.97	12.89	0.7729	Normal
8	2.9	1.82	2.8902	1.6936	3.83	7.43	0.87	14.41	0.8343	Normal
9	2.38	1.9	2.4184	1.7017	3.21	6.55	0.94	13.36	0.7819	Normal
10	6.24	4.27	6.28	3.97	18.43	20.06	0.57	21.83	0.77	Abnormal

REFERENCES

[1]. Usha B S, Sandya S, Shruthi G, "Size and Shape Based Ovarian Abnormality Detection of Ultrasound Images ",ICERECT-12, LNEE, Springer, 10.1007/978-81-322-1157-0_31

[2]. Usha B S, Sandya S, Measurement of Ovarian Size and Shape Parameters,IEEE Xplore, 10.1109/INDCON.2013.6726079

[3]. Usha B S, Sandya S, Ultrasound Ovary Image Classification Using Kσ-Classifier, BME-2014, Ho Chi Minh City, Vietnam.

[4]. Carlo Tomasi and Roberto Manduchi, "Bilateral filtering for gray and color images," in Computer Vision, 1998. Sixth International Conference on . IEEE, 1998, pp. 839– 846.

[5]. Pietro Perona and Jitendra Malik (July 1990). "Scale-space and edge detection using anisotropic diffusion". IEEE Transactions on Pattern Analysis and Machine Intelligence, 12 (7): 629–639. doi:10.1109/34.56205.

[6]. Y. Yu, S. T. Acton, and S. Member, "Speckle Reducing Anisotropic Diffusion," IEEE Transactions On Image Processing, vol. 11, no. 11, pp. 1260–1270, 2002, 88DOI 10.1109/TIP.2002.804276

[7]. Zuiderveld, Karel. "Contrast Limited Adaptive Histograph Equalization." Graphic Gems IV. San Diego: Academic Press Professional, 1994. 474–485.

[8]. P.S.Hiremath and Jyothi R. Tegnoor, Follicle Detection in Ultrasound Images of Ovaries using Scanline Thresholding Method

[9]. P.S.Hiremath and Jyothi R. Tegnoor, "Recognition of Follicles in Ultrasound Images of Ovaries using Geometric Features" IEEE Transactions On Medical Imaging Vol. 17, No. 6 978-1-4244-4764.

Rehabilitation of the Blind using Audio to Visual Conversion Tool

Ashwani Kumar Aggarwal
Electrical and Instrumentation Engineering Department, SLIET, Longowal, Sangrur, Punjab, INDIA
ashwani_75@yahoo.com

ABSTRACT

In human beings, eyes play a vital role. A very less research has been done for rehabilitation of blindness for the blind people. This paper discusses the work that helps blind people for recognizing the basic shapes of the objects like circle, square, triangle, horizontal lines, vertical lines, diagonal lines and the wave forms like sinusoidal, square, triangular etc. This is largely achieved by using digital camera, which is used to capture the visual information present in front of the blind person and a software program, which achieves the image processing operations, and finally the processed image is converted into sound. After the sound generation process, the generated sound is fed to the blind person through headphones for visualizing the imaginary image of the object. For visualizing the imaginary image of the object, it needs to train the blind person. Various training process methods had been applied for recognizing the object.

Keywords: Image processing, Pixel, Pitch, Loudness, sound generation, Edge detection, brightness

1. INTRODUCTION

In human beings Eyes will play vital role. Generally the vision impairment caused due to several reasons such as blindness by birth, various damages to the brain etc[1]. In order to help blind people various instruments had been developed for rehabilitation of blindness [2]. But still the developed instruments are not satisfactory for the rehabilitation of blindness [3]. The present work aims at the rehabilitation of the blind person to recognize the basic shapes of the objects, because in the universe every object has some shape that is the combination of the basic shapes like Circle, Square, Triangle, Horizontal lines, vertical lines, Diagonal lines etc. This is achieved by, the visual information present in front of the blind person is captured by using a digital camera, later the acquired image is undergone various image processing techniques and the processed image is converted into sound. By listening to the sound patterns the blind

person has to visualize the imaginary image of the original object. The block diagram of the system and sound generation process is explained in the following sections of this paper. After the sound generation process, it needs to train the blind person for recognizing the objects. After training the blind person, more than 80% of the results are satisfactory. Before going to the inner details of the work, the fundamentals of the digital image and digital audio have been discussed.

1.1   Fundamentals of a Digital Image

A Digital Image is defined as rectangular array of dots called Pixels [4]. Each digital image is comprised of many pixels and each pixel has its own color. High quality Image in general requires more pixels than low quality images. Generally digital images can be produced as Black & White, Grayscale and color. The color information in the pixel is represented in terms of the Bit depth of an image. Bit depth is defined as the number of bits used to define each pixel[5].

1.2   Introduction to Digital Audio

Sound is what we experience when the ear reacts to a certain range of vibrations, such as a guitar string. As the string moves in one direction, it pushes on nearby air molecules, causing them to move closer together. This creates a small region of high pressure on one side of the string and low pressure on the opposite side. As the string moves in opposite direction, the areas of high and low reverse [6].
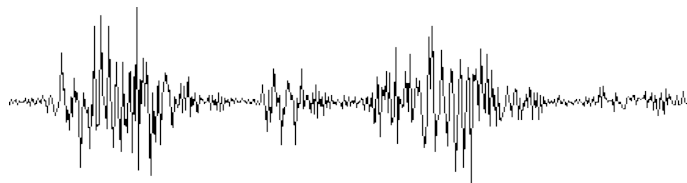
Figure 1.2 A sample Analog Sound Signal

The Sono Visualization aims the blind person to recognize the basic shapes of objects like Horizontal Lines, Vertical lines, diagonal lines, circle, square, triangle etc by listening sound, because in the universe every object has some shape that is the combination of basic shapes. By listening sound patterns the blind person has to visualize the imaginary image of the original object present in the image [7]. For visualizing the imaginary shapes of the objects it needs to train the blind person.

2. IMAGE TO SOUND CONVERSION

Different sinusoidal oscillators form an orthogonal basis, assuming they have frequencies that are integer multiples of some basic frequency [8]. A pixel at a more elevated position i corresponds to an oscillator of higher frequency f_i. The larger the brightness of a pixel represented by gray tone , the larger the amplitude ("loudness") of its associated oscillator [9].
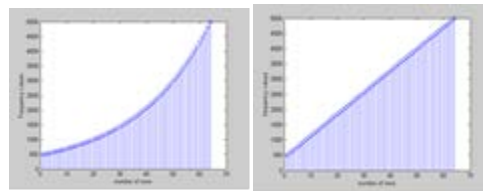
The M oscillator signals for the single column are superimposed, and the corresponding sound pattern s(t) is presented to the ear during T/N seconds. Then the next, (j+1)th, column, is converted into sound: this procedure continues until the rightmost, Nth, column has been converted into sound, T seconds after the start of the conversion.   For a given column j, every pixel in this column is used to excite an associated sinusoidal oscillator in the audible frequency range. For 64 x 64 pixel matrix, M = 64 behavior of sinusoidal oscillators are implemented digitally, whose frequency values of sinusoidal waves is calculated by using exponential or Equidistant frequency distributions, amplitude of the sine waves is calculated by using color (brightness) of the pixels and the phase values are generated randomly in the range of 0 to 1. The phases   are just arbitrary constants during the image to sound conversion process [10]. The ear is insensitive to phase because it contains little useful information. But we cannot say that the ear is completely deaf to phase because a phase change can rearrange the time sequence of an audio signal [11]. Once in a column after processing of the entire pixel information then mix all the signals produced in a column. Then increment the column and repeat the process until the last column. All the sound samples, which are generated, are written to the wave file by adding the header [12].

3. RESULTS

In the Sono-Visualization system, all the algorithms were developed in C language by using VC++ Compiler 6.0. The input color JPEG images were generated either with Microsoft paint or by using Logitech web camera, which was then converted into BMP grayscale image [13]. Some of the input images and the corresponding output images are shown below. Once after the sound generation, the sound was fed to the blind person through headphones.

Table 1: Results of Horizontal, Vertical and Diagonal Lines

Time of the sound file Played in sec	1 horizontal line	2 horizontal lines	3 horizontal lines
2.10	Y	N	N
5.25	Y	N	N
10.50	Y	Y	N
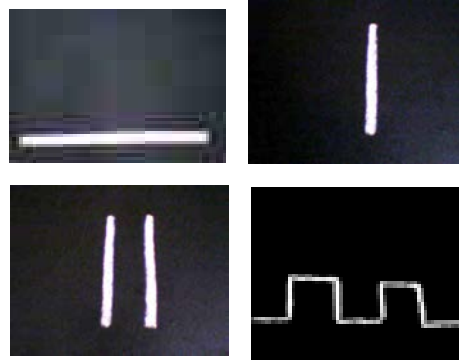
Figure 1: The input image containing a Square wave
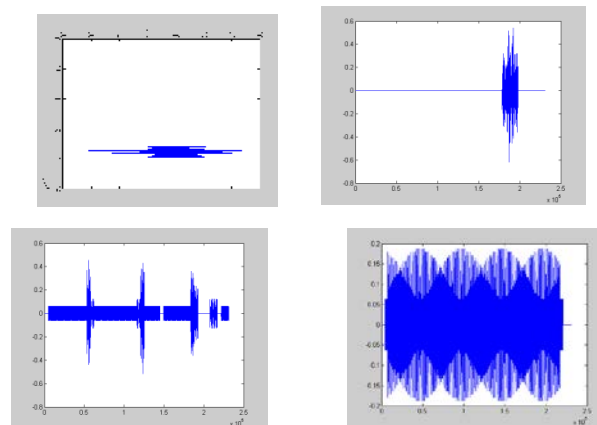
Figure 2: Output wav sound file graph.

For recognizing the object it needs to train the blind person [14]. Various procedures have been applied for training the blind person. The present work had chosen the blind persons with the age in the range of 15-20 years. First the blind person was trained with horizontal, vertical, diagonal lines and then to square, circle, triangle etc and then to other complicated structures. The results are shown in the tabulated form. If the blind person recognized the object then it is represented as 'Y' stands for 'Yes' otherwise 'N' for 'No'

The blind person is able to recognize the vertical lines in short period of time. The blind person is able to recognize the vertical lines in minimum period of time [15].

The blind person was able to recognize the single horizontal line in an image, but in case of 2 to 3 horizontal lines, the person told some multiple lines were there so he was not able to trace the exact number of ones. In minimum time period the blind person was not able to trace the both the up & down diagonal lines. But with increase of time the person had recognized both the shapes.

4. COMMENTS AND DISCUSSION

Here first the blind person was trained with the various basic shapes and the random shapes of sound files are played for recognition. In minimum time period the blind person was

in confusion to recognize the object, but with increase of time the person had recognized successfully. With the available feedback, the blind persons were then trained with the combination of the above mentioned shapes like combination of horizontal and diagonal, diagonal and vertical etc. Here also the results are satisfactory, they recognized the combination of the shapes also.

In next phase the blind persons were trained with the waveforms like sine waves, triangle waves, square pulses, saw tooth waves etc. This had taken more time to recognize the wav forms. But the results still are satisfactory.

The blind persons visualized the vertical lines easily and they were able to tell how many vertical lines were there in the image. But in case of horizontal lines, they were able to recognize the horizontal line but not able to recognize how many lines were present. Even the sound file playing time was increased to 10 seconds; they were hardly able to recognize the number of lines. But more than 80% of the results are satisfactory. Even the combination of the shapes was also recognized. For more effective recognition if we generate the stereo sound, it would help the blind person to recognize the direction of the object i.e. whether it is there on right or left. For recognizing the complicated shapes it needs a lot of training and the blind person has to use this tool daily.

5. CONCLUSION

The Sono Visualization Blind Aid Tool is developed to help blind people in recognizing the basic shapes of the objects like circle, square, rectangle, horizontal, vertical and diagonal lines etc. The blind persons trained with these basic shapes, with less effort that they easily recognized the basic shapes. With continuous training they can be able to recognize the multiple objects and combination of the objects. The main important aspect in this is the sound generation process. The sound is generated by simple mapping of the image properties into sound properties. Sound is generated in the form of simple sinusoidal wave forms. The mono type sound is generated by adding the wav header file to the sound samples for playing the sound file. Wav file format is used because it is the windows operating system most favorable format. Edge detection of the image and conversion of the JPEG to BMP image conversion are provided as an optional for user convenience [16]. Edge detection helps the blind person to recognize the solid shapes of the objects. JPEG to BMP conversion procedure is used for user compatibility to work with both JPEG and BMP image files[17].

6. FUTURE SCOPE OF THE WORK

6.1   Generation of Stereo sound

The present work generates the Mono type sound form; in advanced version to recognize the objects more effectively stereo sound is generated. Stereo sound helps the blind person to recognize the objects easily [18] whether it is there on right or left. If the object is there on right, the generated sound will first reach the right ear and vice versa. The stereo sound is generated in wav file format with 16-bit resolution [19]. Scanning is simultaneously carried out on the first column and last column of the image. After this scanning procedure, the generated sound is outputted to the headphones. The procedure is implemented until the centerline of the image is met. Sound will be produced after every simultaneous scanning of the two-mirrored columns in each image[20].

6.2   Developing of prototype and Mobile based system

In order to work in the real time environment a prototype system is developed, which consists of a head mounted digital camera, a suitable DSP system to achieve image processing and sound generation process are assembled with the headphones. The system should be portable, should be run on battery operated and should have low power consumption capability[21]. The system can be developed on a Mobile based device as the Digital cameras with built in camera are available easily in the market at low cost. The visual information present in front of the blind person is captured by using built in camera of a mobile phone and a suitable software program generates the sound. The generated sound is then fed to the blind person through head phones to visualize the imaginary image of the original object. The software program is made to run by using either Symbian or Nucleus operating system [22].

6.3   Encoding of the sound in the form of MIDI and MP3

In general it is difficult to recognize the normal sounds for reorganization of the objects. To overcome this problem the normal sounds are encoded in the form of MIDI (Musical Instrument for device interfacing). The human beings can easily grasp the music compared to the normal sounds. For different objects different sounds of instruments are to be encoded, for example if we encode the piano sound for an object, if the object is located at high then the intensity of the piano music is more and vice versa. Encoding the sound into music helps the blind person to recognize the object more easily.The present work generates the sound in the form of wav file format. But the disadvantage with the wav files is the size of the file is very large and it is in the uncompressed format. It will occupy more memory space, this is a major problem when the system is developing on mobile based, because in the mobile based devices have the limited memory. To overcome this problem the sound is generated in the form of MP3, which is compressed format and the size of the file is very less. The MP3 sound is generated by using Wav to MP3 encoding procedure [23].

6.4   Further future scope of the work

The further future scope of this work aims the blind person to recognize the color of the object, whether the object is red or green or blue, size of the object whether it is large or small. For reading the text like alphabets and numbers is also achieved with the help of Optical character recognition (OCR) machine, to recognize the characters. After that by using a speech synthesizer it will say the name of the alphabet or number like A, C, D or 1, 2, 3. The output of the speech synthesizer is fed to the headphones of the blind person for reading the text.

ACKNOWLEDGMENT

REFERENCES

[1].   Gonzalez R.C. and Woods Richrd. E "Digital image processing" second edition, published by Pearson education. Pte.led., pp 54-62, March-2003.

[2].   B.Thylefors, A.-D. Negrel, R. Paramjasegaram and K.Y. Dadzie, " Global Data on blindness", *Bulletin of the world health organization* 73(1), pp.115-121,1995.

[3].   Tohru Ifukube, Tadayuki Sasaki and Chen Peng, "A Blind Mobility Aid Modeled after echo-location of Bats" *IEEE Trans. Biomed. Eng.,* Vol.38, pp.461-465, May 1991.

[4].   S. Shoval, J. Borestein and Y. Koren, " The NAVBELT – a computerized Travel Aid for blind Based on Mobile Robotics Technology", *IEEE Transactions on Biomedical Engneering*Vol.45, No.11,pp. 1376-1386, November 1998.

[5].   F.Wong, R.Nagarajan, S.Yaacob, A.Chekima and N-E. Belkhamza, " Electronic Travel Aids for Visually Impaired – a Guided Tour", proceedings of conference in Engineering in Saraw-ark In the Last century and for the Next Decade, Kuching, Sarawak, pp. 111-129, May 2000.

[6].   L.Kay, " A sonar aid to enchance spatial perception of the blind: Engineering, design and evaluation," Radio, Electron, Engineer, vol.44, pp.605-627, 1974.

[7].   Brabyn, J., Crandall, W., Gerrey, W., "Talking signs: a remote signage, solution for the blind,visually impaired and reading disabled" Engineering in Medicine and Biology Society, Proc-eedings of the 15th Annual International Conference of the *IEEE* Oct 28- 31, 1993 Page(S): 1309 – 1310.

[8].   C. Capelle, C.Trullemans, P.Arno and C.veraart, "A Real Time Experimental prototype for Enhancement of vision rehabilitation using Auditory Substitution", *IEEE Transactions onBiomedical Engineering,* vol.45,No.10, pp 1279-1293, October 1998.

[9].   Meijer, P.B.L., "An Experimental System for Auditory Image Representations"*, IEEE Trans. on Biomedical Engineering,* Vol.39, No.2, pp.112-121, February 1992.

[10].   Wm. H. Dobelle, "Artificial Vision for the Blind by Connecting a Television Camera to the Visual Cortex" *ASAIO Journal 2000; 46:3-9.*

[11].   Cronly-Dillon, J.,Persaud, K. C., Blore, R., (2000) "Blind subjects construct conscious men tal images of visual scenes encoded in musical form." *Proceedings Of The Royal Society London Series B-Biological Sciences*, *267,* 2231-2238.

[12].   Matta, S., Kumar D. K., Xinghuo Yu, Burry M, "Discriminative Analysis for Image to sou- d Mapping" Intelligent sensing and information processing, 2004. Proceedings of internat- ional conference on 2004 page(s);119-122.

[13].   J. Dowling, A. Maeder and W. Boles, ``Intelligent Image Processing Constraints for Blind Mobility Facilitated through Artificial Vision,'' *Eighth Australian and New Zealand Inteli gent Information Systems Conference* (ANZIIS 2003), Sydney, Australia, pp. 109-114, December 10-12, 2003.

[14].   R. Nagarajan, S. Yaacob and G. Sainarayanan, ``Role Of Object Identification In sonofication System For Visually Impaired,'' *IEEE Tencon 2003* ("IEEE Region 10 Conference on Convergent Technologies for the Asia-Pacific"), October 15-17, 2003, Bangalore, India.

[15].   Gonzalez R. C. and Woods R. E "Digital image processing" second edition, published by Pearson education.Pte.led., pp 38-42, March-2003.

[16].   W.F.Ganong, *Review of Medical Physiology*, 15th ed., Appleton & Lange, Eds. London, U.K.: Prentice-Hall 1991.

[17].   E. Zwicker, "Scaling", in handbook of sensory Physiology, vol, V/2 Auditory system, phy-siology (CNS), Behavioral studies, psychoacoustics, W. D. Keidal and W. D. Neff, Eds. Berlin,Germany: Springer-verlag, 1975.

[18].   Steven W. Smith "The scientist and Engineer's Guide to Digital signal processing" second edition published by California Technical Publishing, pp.351-370., chapter 22 –Audio Proc.

[19].   G. K. Wallace, "The JPEG still picture compression standard", *Communications of the   ACM*, vol.34, no.4, pp.30-44, Apr.1991.

[20].   Wong, F.; Nagarajan, R.; Yaacob, S.; Chekima, A.; Belkhamza, N.-E.;"A stereo auditory display for visually impaired" TENCON 2000. Proceedings Volume 2, 24 -27   Sept.,2000.,Page(s):377-382,vol.2

Nuclear Magnetic Resonance Spectroscopic Studies of Human Immunoglobulin 'G' in Alzheimer's Disease

Sanjeev Kumar and Shweta chaudhary

*Department of Physics, Medical Physics Research Laboratory, D.A.V. (P.G.) College,
Muzaffar Nagar – 251 001 U.P. (India).*
sanjeev1962kumar@rediffmail.com ; sanjeev1962kmar@yahoo.co.in

ABSTRACT

In the present paper, we have studied human IgG in Alzheimer's disease(AD) using nuclear magnetic resonance spectroscopy. A comparison with normal controls is also made. NMR spectroscopy is a powerful tool to detect the chemical groups of amino acids in serum. According to data available with the present study we are giving some of the findings related to AD patients. A group Aspartic acid (α-CH) is found in four cases only of AD patients and this group was absent in all the normal healthy persons. The group isoleucine (δ-CH$_3$) has been found in all the blood samples of normal persons and AD patients. Glutamic acid (α-CH) is found in two cases of AD patients and was absent in all the normal persons and other patients of AD. Alanine (β-CH) is found in two cases of normal healthy people and four cases of AD patients only. Asparatic acid (α-CH) is found in four cases of AD patients only and absent in all the normal healthy people. Lysine (γ-CH$_2$) is found in one case of AD patient only and absent in all the normal healthy controls along AD patients. Isoleuicine ($\gamma-$ CH$_3$) has been found in three cases of AD patients only and four normal healthy people. Cystine (α-CH) and Cystine (β-CH) have been found in two cases of AD patients only and absent in all the normals with AD patients. Tryptophane (α-CH) is found in two sample of AD patient only and absent in all the cases of AD and normal healthy people . The appearance or disappearance of NMR groups may be changes in the CNS due to alteration in trace elements and immunity

Keywords : Chemical shift (δ) , gyromagnetic ratio (γ), Nuclear Magnetic Resonance (NMR), Immunoglobulin G (IgG) and Alzheimer's disease (AD)

1. INTRODUCTION

Nuclear magnetic resonance (NMR) technique of spectroscopy is a next step of X-ray crystallographic studies. NMR may provide high resolution structure of biological molecules. These molecules are proteins and nucleic acids and their complexes at atomic resolution.

The first application of nuclear magnetic resonance (NMR) spectroscopy to a biological sample was performed by Jacobson, B. et.al. [1] in 1954. Saundrer, S. M. et. al. [2] have applied this spectroscopy at 40 MHz to protein, ribonuclease. Some of the authors [3-6] have given useful information related to structure of biological macromolecules.

The magnetic resonance phenomenon occurs as a result of the quantum mechanical property of spin. We may presume that this is a source of angular momentum intrinsic to a number of different nuclei. Spin angular momentum confers a magnetic moment on a nucleus. The nuclear spin (I) can have the values of I as 0, ½, 1, 1½ + ... etc.

Some biological nuclei such as 12C and 16O have zero nuclear spin and do not give NMR spectra.

Nuclear magnetic moment (μ) is given by

$$\mu = \quad \square\, I\, \square \qquad\qquad (1)$$

The gyromagnetic ratio $\square$ is the propo frequency of the nucleus for a given external field. Magnetic properties of some biologically useful nuclei are given in table 1. A nucleus of spin I in a magnetic field has 2I +1 possible orientations. These orientations are given by the value of the magnetic quantum number (mI), which has value of − I, −I + 1, - - - I−1). If a nucleus by a spin 3/2 then the magnetic quantum number has the value such as –3/2, –½, ½, 3/2. We can use a nucleus of spin –1½ as a bar magnet, which varies with orientations to the field. The possible energies are quantized, with the two possible valued of mI (± ½) corresponding to parallel and antiparallel orientations to this small magnet and the external field. NMR absorption is a consequence of transitions between the energy levels stimulated by applied radio frequency (RF) radiation.

Nuclear spin has quantized nature. We can describe the motion of a nucleus in a magnetic field in terms of classical mechanics. In the presence of an applied magnetic field , the magnetic moment experiences a torque which is the vector product of the nuclear angular momentum and the magnetic moment . Schematic presentation of the motion of a nucleus in a magnetic field is given in fig. 1. Magnetic properties of some biologically useful nuclei is given in Table 1.

Physical picture is not a real picture and unable to show any reality. The findings of Stern-Gerlach experiment suggest that spin angular momentum is quantized. Classical mechanics failed here. The nucleus is not necessarily spinning about its axis. It may spin radial velocity with the speed of light. Magnetic moment is a purely quantum mechanical property.
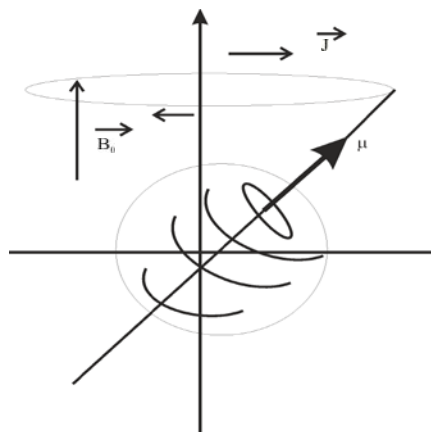
Fig. 1. Schematic presentation of the motion of a nuclees in a magnetic field.

Table 1. Magnetic properties of some biologically useful nuclei

Isotope	Spin	Natural abundance(%)	Quadrupole moment Q (10^{-28} m^2)	Gyromagnetic ratio Y (107 rad s^{-1} T^{-1})	Sensitivity rel.[a]	abs.[b]	NMR-frequency (MHz) at a field (T) of 2.3488
^{1}H	1/2	99.98	-	26.7522	1.00	1.00	100.000
^{2}H	1	1.5×10^{-2}	2.87×10^{-3}	4.1066	9.65×10^{-3}	1.45×10^{-6}	15.351
^{3}H	1/2	0	-	28.5350	1.21	0	106.663
^{7}Li	3/2	92.58	-3.7×10^{-2}	10.3976	0.29	0.27	38.863
^{11}B	3/2	80.42	4.1×10^{-2}	8.5847	0.17	0.13	32.084
^{13}C	1/2	1.108	-	6.7283	1.59×10^{-2}	1.76×10^{-4}	25.144
^{14}N	1	99.63	1.67×10^{-2}	1.9338	1.01×10^{-3}	1.01×10^{-3}	7.224
^{15}N	1/2	0.37	-	-2.7126	1.04×10^{-3}	3.85×10^{-6}	10.133
^{17}O	5/2	3.7×10^{-2}	-2.6×10^{-2}	-3.6280	2.91×10^{-2}	1.08×10^{-5}	13.557
^{19}F	1/2	100	-	25.1815	0.83	0.83	94.077
^{23}Na	3/2	100	0.10	7.0704	9.25×10^{-2}	9.25×10^{-2}	26.451
^{25}Mg	5/2	10.13	0.22	-1.6389	2.67×10^{-3}	2.71×10^{-4}	6.1195
^{31}P	1/2	100	-	10.8394	6.63×10^{-2}	6.62×10^{-2}	40.481
^{35}Cl	3/2	75.53	-8.2×10^{-2}	2.6242	4.70×10^{-3}	3.55×10^{-3}	9.798
^{39}K	3/2	93.1	5.5×10^{-2}	1.2499	5.08×10^{-4}	4.73×10^{-4}	4.667
^{43}Ca	7/2	0.145	-5×10^{-2}	-1.8028	6.40×10^{-3}	9.28×10^{-6}	6.728
^{51}V	7/2	99.76	2.17×10^{3}	-5.2×10^{-2}	0.38	0.38	26.289
^{57}Fe	1/2	2.19	-	0.8687	3.37×10^{-5}	7.38×10^{-7}	3.231
^{75}As	3/2	100	0.29^{u}	4.5961	2.51×10^{-2}	2.51×10^{-2}	17.126
^{77}Se	1/2	7.58	-	5.1214	6.93×10^{-3}	5.25×10^{-4}	19.067
^{113}Cd	1/2	12.26	-	-5.9609	1.09×10^{-3}	1.33×10^{-3}	22.182

a   At constant field for equal number of nuclei.

b.   Product of relative sensitivity and natural abundance.

According to Newtonian mechanics, this torque equals the rate of change of angular momentum.

$$\frac{d\vec{J}}{dt} = \vec{\mu} \times \vec{B_o} \tag{2}$$

$$\vec{J} = \vec{I}\,\hbar \tag{3}$$

$$\frac{d\vec{\mu}}{dt} = \gamma\vec{\mu} \times \vec{B_o} \tag{4}$$

The equation (4) is analogues to the equation of motion for a body with angular momentum $\vec{L}$ in a gravitational field $\vec{g}$ with mass m at a distance $\vec{r}$ from the fixed point of rotation, if we equate $\vec{J}$ to $\vec{L}$ and $\vec{B_o}$ to $\vec{g}$ and $\vec{r} \times \vec{m}$ as an intrinsic property of the body which is analogous to $\gamma\vec{\mu}$ then we can write rate of change of angular momentum i.e.

$$\frac{d\vec{L}}{dt} = \vec{r} \times m\vec{g} \tag{5}$$

Thus we may see that this is just like the motion of gyroscope, which in a gravitational field processes, i.e. its axis of rotation itself rotates about the field direction. In the classical point of view, the same motion occurs for a nuclear spins in a magnetic field.

The energy of the interaction is directly proportional to $\vec{\mu}$ and $\vec{B_0}$.

$$\therefore \quad E = -\gamma \hbar\, m_I\, \vec{B_o} \qquad \text{and} \qquad \Delta m_I = 1 \tag{6}$$

$$\therefore \quad \Delta E = -\gamma \hbar\, \vec{B_o} \tag{7}$$

and if we apply Planck's law

$$\Delta\vec{E} = h\nu \tag{8}$$

then

$$\nu = \frac{\gamma\vec{B_o}}{2\pi} \text{ (in Hz)} \tag{9}$$

or

$$\omega = -\gamma\, \vec{B_o} \text{ (in rad s}^{-1}) \tag{10}$$

The nucleus precess arround the magnetic field $\vec{B_0}$ axis at a speed, which is called Larmor frequency ω. The rotation may be clock-wise or anticlock-wise depending on the sign of γ. It is same for any particular nucleus. Energy level diagram is shown in figure 2.
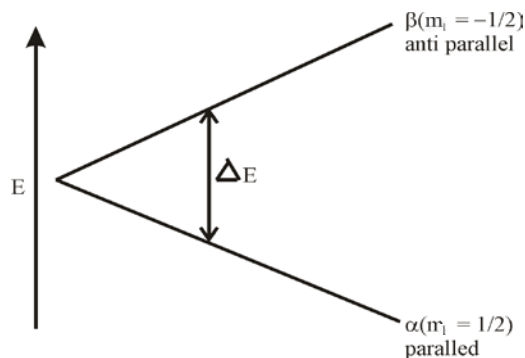

Fig. 2. Energy level diagram.

We have seen that in an energy level diagram there are two energy states α and β. Both of them will be unequally populated. The ratio of these two is given by Boltzmann equation.

$$\frac{N\beta}{N\alpha} = e^{-\Delta E/k_\beta T} \tag{11}$$

We have a large number of spins in a sample. These spins possessing the same Larmor frequency. The parallel orientation of the Z-component of each spin along the $\overrightarrow{B_0}$ direction is of lower energy than the parallel. We have Boltzmann surplus at thermal equilibrium which is shown in figure 3.
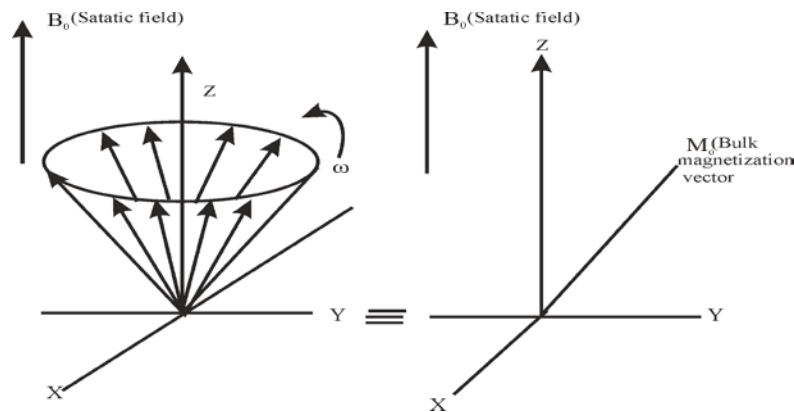

Fig. 3. The bulk magnetization vector.

Thus net magnetization of the sample is along Z axis, which is parallel to the field. All the contributing spins have components precesssing in the xy plane. Due to equal energy of spins the phase of precession is random.

If we call it as an ensemblele of spins. The net magnetization in the xy plane is zero. The total magnetization of the sample is stationary and aligned with the Z axis and it is called $\overrightarrow{M_o}$.

The radio frequency radiation is electromagnetic and can be represented as an oscillating magnetic field. We may represent it as magnetization vectors. Half cycle of oscillation of the magnetization due to the presence of the radio frequency field is called $\overrightarrow{B_1}$ field we can represent it's as two magnetization vectors of constant amplitude rotating about an axis (X) in opposite direction with angular frequency which is equal to radio frequency .A pair of counter – rotating vectors is a way of representing the radio frequency .

The behaviour of the macroscopic magnetization and effects due to relaxation may be understood in terms of model and a mathematical formalism . Bloch, F. [7] has given some information on the magnetic resonance. The method of magnetic resonance has been applied to measure the magnetic moment of the neutral particle i.e. neutron. It has been established that the magnetic resonance was also applied to different types of nuclei. The main feature of this method is the observation of transitions, caused by resonance of an applied radio frequency field with the Larmor precession of the moments around constant magnetic field. Phillips, W. D. [8] has given a detailed theory of magnetization. The complete Bloch equations

are a set of phenomenological differential equations that describes the motion of $\overrightarrow{M}$ in the presence of a static magnetic field directed along the Z axis is $\overrightarrow{H_o}$ and a field constantly rotating in the xy plane is $\overrightarrow{H_1}$. The free spins in a magnetic field possess a nuclear spin angular momentum. The time rate of change of this angular momentum, related to Larmor frequency is given here.

$$\frac{d\overrightarrow{M}}{dt} = \gamma_N \overrightarrow{M} \times \overrightarrow{H} \tag{12}$$

Here $\qquad \overrightarrow{H} = \overrightarrow{H_o} + \overrightarrow{H_1}$.

In a static field directed along the Z-axis the approach of the Z-component of magnetization M_Z, towards its equilibrium value, M_o can be described by a first order process, which is given below

$$\frac{dM_Z}{dt} = \frac{(M_Z - M_o)}{T_1} \tag{13}$$

T_1 is the characteristic spin lattice relaxation time.

If a perturbation of the magnetization produces components M_x and M_y at right angles to the static field, the decay of these components to zero at equilibrium can be described by another first order rate process given by

$$\left. \begin{array}{l} \dfrac{dM_Z}{dt} = \dfrac{-M_Z}{T_2} \\[2mm] \dfrac{dM_y}{dt} = \dfrac{-M_y}{T_2} \end{array} \right\} \tag{14}$$

where T_2 is the characteristic spin-spin relaxation time. T_1 and T_2 are referred to as the longitudinal and transverse relaxation times, with reference to time constants for the decay of magnetization components either parallel or perpendicular to the static field. Bloch combined the above features in a unique way by assuming that the motion of the magnetization due to relaxation could be superimposed on the motion of the free spins.

$$\frac{d\overrightarrow{M}}{dt} = \gamma_N \overrightarrow{M} \times \overrightarrow{H} - \frac{M_x \vec{i} + M_y \vec{j}}{T_2} - \frac{(M_z - M_o)\vec{k}}{T_1}$$

where i, j and $\vec{k}$ are unit vectors directed along the x, y and z axes respectively. The respective components of the magnetization assume a time dependence described by the complete Bloch equations'.

$$\left.\begin{array}{l} \dfrac{dM_x}{dt} = \gamma_N(M_y H_y - M_z H_y) - \dfrac{M_x}{T_2} \\[2mm] \dfrac{dM_y}{dt} = \gamma_N(M_z H_x - M_x H_z) - \dfrac{M_y}{T_2} \\[2mm] \dfrac{dM_z}{dt} = -\gamma_N(M_y H_z - M_x H_y) - \dfrac{(M_z - M_o)}{T_1} \end{array}\right\} \qquad (14)$$

If ω is the angular frequency of $\vec{H_1}$.

The Bloch equations contain terms that refer to the directional components of the static and rotating fields. These components are given below.

$$\left.\begin{array}{l} H_x = H_1 \cos \omega t \\ H_y = -H_1 \sin \omega t \\ H_z = H_o \end{array}\right\} \qquad (15)$$

These relationships were developed using a fixed coordinate system called the laboratory frame of reference.

A reasonable macroscopic explanation of magnetic resonance absorption can be obtained by the further analysis of these equations, which can predicts resonance line shapes. If a coordination system rotates about $\vec{H_o}$ in the direction of the precession of nuclei. This coordinate system can be referred to as the rotating frame of references. If the new coordinate system rotates about Z axis with an angular velocity ω' the useful relation is given below.

$$\left(\frac{d\vec{M}}{dt}\right)_{rot} = \gamma_N \vec{M} \times \vec{H}_{eff} \qquad (16)$$

Here $$\vec{H}_{eff} = \vec{H} + \frac{\vec{\omega'}}{\gamma_N} \qquad (17)$$

Study of One dimensional Nuclear Over Hauser (NOE) effects.

Nuclear over Hauser effect is the change in the integrated intensity of an NMR signal from a nuclear spin when a neighboring spin is saturated. It is very difficult to measure the internuclear distances (r_{ij}) in solution. NOE makes it better to measure r_{ij} in solution. NOE has been extensively used to study of configurations of biologically macromolecules.

The measured signal in an NMR experiment is free induction decay a (FID). If we do not have noise in signals then the free induction decay can be represented as

$$M(t) = \vec{M_o} \cos(\omega_o t)\, e^{-t/T_2} \qquad (18)$$

where M_o is inital magnetization ω_0 is the carrier frequency, T_2 is an effective spin-spin relaxation time.

We can use fourier transform form of magnetization M(t), which is given below.

$$\hat{M}(\omega) = \int_{\ell}^{\infty} M(t)e^{-i\omega t}dt \tag{19}$$

using equation (18) and taken real parts only equation (19) we get.

$$\hat{M}(\omega) = \vec{M_o}T_2 \Big/ \Big[1 + (\omega - \omega_o)^2(T_2)^2 \Big] \tag{20}$$

The equation (20) shows a Lorentzian curve centered at $\omega = \omega_0$.

Area under the Lorentzian peak in equation (20) is given by the equation, which is given below

$$\int_{-\infty}^{+\infty} \hat{M}(\omega)\,d\omega = \pi\vec{M_o} \tag{21}$$

If $\pi\vec{M_o}$ is the area under the peak in the absence of a saturating radio frequency (RF) field.

If $\pi M'_o$ be the area of peak in the presence of a saturating RF field applied to the resonance of a neighbor nucleus.

NOE is defined in terms of the relative difference between two peak areas

$$\eta = (M'_o - M_o)\big/M_o \tag{22}$$

$$NOE = 1 + \eta \tag{23}$$

The value of NOE is related to molecular parameters of interest, which is given below

$$NOE = f(\tau_c)/r^6ij \tag{24}$$

where $f(\tau_c)$ is a function of the rotational correlation time that depends on the model under consideration rij is the distance between the nucleus whose peak area is being measured and the nucleus is being strongly irradiated. NOE is defined as a measure of change in the steady state description of a nuclear spin system resulting from an external disturbance.

Chemical Shifts:

We are discussing about an important property of NMR i.e. chemical shift, which is one of the most basic parameters of this technique of spectroscopy. It is generally defined as δ in parts per million (ppm) and given by the relation

$$\delta = \frac{\omega - \omega_o}{\omega_o} \times 10^6 \tag{25}$$

where ω_0 is Larmor frequency in Hz and ω is the resonant frequency of the line of interest.

We can use $\omega - \omega_o$ as Ω. The origin of the chemical shift is that the moving electric charge of the electron cloud around a nucleus induces a local magnetic field, which opposes the applied field. The effective field at the nucleus is given by

$$\vec{B}_{eff} = \vec{B}_o(1-\sigma) \tag{26}$$

Thus the nucleus is said to be shielded, and the extent of the shielding is given by the shielding constant. It is also called the chemical shift tensor 'σ'. This is directly related to the electron density ρ at a distance $\bar{r}$ from the nucleus and given by Lamb's equation.

$$\sigma = \frac{4\pi e^2}{3me^2} \int_{-\infty}^{+\infty} r\rho(\bar{r})dr \tag{27}$$

There are three principal components of the shift tensor, i.e. σ_{11}, σ_{22}, σ_{33}. The isotropic shift tensor σ_{iso} is given by

$$\sigma_{iso} = 1/3 \ (\sigma_{11} + \sigma_{22} + \sigma_{33}) \tag{28}$$

The shift tensor σ is related to Larmor frequency ω as

$$\omega_o = \frac{\gamma}{2\pi}\vec{B}_o(1-\sigma) \tag{29}$$

and σ is related to chemical shift as

$$\delta = 10^6(\sigma_{ref} - \sigma_{sample}) \tag{30}$$

Linden, J. C. et. al. [9] have studied this technique and given a brief introduction of investigations on biofluids. Investigation of biofluids composition provides insight the status of a living organism in that the composition of a particular fluid carries biochemical information on different types of modes and severity of organ dysfunction. NMR analysis of biological fluids is a best approach these days.

Due to enormous complexity of the matrix complete assignment of ^{1}H NMR spectrum of most biofluids is not possible even at 900 MHz NMR. However, the assignment problems vary considerably among biofluids. Seminal fluid and blood plasma are highly regulated with respect to metabolic composition and concentrations. We can receive majority of NMR signal at 750 MHz for normal human beings. Urine composition is more variable because its composition is adjusted by the body in order to maintain homoeostasis. Total analysis of urine is very difficult. There are so many fluctuations in the concentration range of NMR detectable metabolites in urine samples. All biological fluids have their own characteristic physiochemical properties. NMR is not suitable for detection of some important biochemical substances for example hormones, we can study complex biomixtures with the help of NMR spectroscopy. NMR spectroscopy of biofluids is well established for probing a wide range of biochemical perturbations. We have many physiochemical phenomena in biofluids. Subtle interactions

occurring between macromolecules and small molecules. It is now hundred percent possible to study enzyme reactions, chemical reactions and biofluids instability, microbiological activity in biofluids, macromolecular binding of small molecules, membrane-based compartmentation, metal complexation and chemical exchange processes.

Biochemistry of blood and its various cellular components and plasma have been extensively studied by NMR spectroscopy. The physical properties of whole blood impose very serious limitations on direct NMR investigations. Erythrocytes in packed form yield more useful information on cell biochemistry. NMR measurements on blood plasma and serums can provide very useful biochemical information on both low molecular weight metabolites and macromolecular structure and organization, NMR peaks of metabolites; proteins, lipids and lipoproteins are overlapped in blood plasma. Most of the blood plasma samples are very viscous and due to this property of blood short T_1 relaxation times for small molecules occur. We can get short pulse repetition cycle without signal saturation. We can simplify spectral profile by applying spin-echo experiments with suitable T_2 relaxation delay to allow signals from broad macromolecular components and compounds bound to proteins to be attenuated. The signals from some lipid and lipoprotein components such as very low density lipoproteins (VLDL), low density lipoprotein (LDL), high density lipoprotein (HDL) have been partially characterized. Lipoproteins are complex particles that transport molecules normally insoluble in water. They are spherical with a core region of triglyceride and cholesterol ester lipids surrounded by phospholipids in which are embedded so many proteins called apoliporoteins. Free cholesterol is available in core and surface regions. Lipoproteins are in a dynamic equilibrium with metabolic changes going in vivo. ^{1}H NMR spectroscopy is useful in lipoprotein analysis and ^{31}P NMR spectroscopy is used to study phospholipids in blood plasma. Neural network software approach has been extensively used to provide a rapid analysis of lipoproteins.

Blood sugar is a common problem these days, which can be more serious and complex if it is not treated properly. This symptom is characterized by polyurea, weight loss in spite of increased appetite, high plasma and urinary levels of glucose, metabolic acidosis, ketosis and coma. The muscles and other tissues demanded more and more glucose. Elevation of glucose levels are found in urine and plasma. NMR spectra showed a marked elevation in plasma levels of ketone bodies and glucose.

The CH_3 and CH_2 resonances of lipoproteins VLDL and chylomicrons were decreased significantly in intensity relative to CH_3 signal of HDL and LDL, which indicates that the rapid metabolism of the mobile pool of triglycerides in VLDL and chylomicrons. On the basis of NMR technique spectra of CSF of different diseases such as lumbar disk herniations, cerebral tumors, drug over dose, diabetes, hepatic encephalitis, multiple sclerosis, AIDS, dementia Parkinson's disease, Creutzfeld-Jakob disease, Guillain-Barre syndrome and Vitamin B_{12} deficiency.

NMR spectra of seminal fluid has also been recorded at 750 MHz ^{1}H NMR and found that many of signals have been assigned with very broad and poorly resolved signals due to presence of high concentrations of peptides. The complexity of the biochemical composition of seminal fluids together with their reactivity poses a number of assignment and quantitative measurement problems. Studies of infertility include a method, which provides automatic diagnosis based on NMR spectroscopy. 31P NMR spectroscopy has also been used to distinguish semen from healthy and infertile men.

Some metabolic signals in seminal fluids also appear to have irregular chemical shifts in comparison to other body fluids. A number of studies have used 1H and 13C NMR spectroscopy of bile to aid characterization of its composition and structure. 13C spectra of bile from fish exposed to petroleum have been studied. 31P NMR spectra of human bile have also been studied. 1H NMR spectroscopy of bile has been used to investigate the micellar cholestrol content and lipids. 1H and 31P NMR spectroscopy have been used to study the distribution of lecithin and cholesterol. To monitor liver function 1H NMR spectroscopy of bile may be used . 31P NMR spectra of bile from patients with primary biliary cirrhosis of the liver and from clinically healthy men have been studied. 1H NMR spectroscopy has been extensively used to study the bile in hepatobiliary disease ,which includes cancer and the levels of lactate in bile have been estimated.

1H NMR spectroscopy has been used to study human amniotic fluid and detected eighteen small molecule metabolites including glucose, leuicine, isoleuicine, lactate and creatinine. The effect of different pathological conditions during pregnancy has been investigated using 1H NMR spectroscopy of human amniotic fluid. 31P NMR spectroscopy has been applied to study the phosphorous content in amniotic fluid. Some nuclear magnetic resonance spectral studies of metabolic profiling of ovarian follicular fluids from sleep pigs and cow have been established. 19F NMR spectroscopy has been used to defect trifluoroacetic acid in milk.

1H NMR spectroscopy has been applied to measure the levels of different types of endogenous components in the synovial fluid ,which was taken out from the knees of the patients of osteoarthritis, rheumatoid arthritis and traumatic effusions. The low molecular weight endogenous components showed a wide patient to patient variability and showed no statistically correlation with disease state. It has been established that the correlations with the the disease states and the synovial fluid levels of the N-acetyl signals from acute phase glycoprotein's.

Correlations between the disease state and the levels and type of triglyceride in the synovial fluid have been studied earlier.

13C NMR spectroscopy used to monitor the synovial fluids from patients with arthritis. 1H NMR spectroscopy supplied more information of signals from hyalcronic acid, which is the main determinant of the viscoelasticity of the synovial fluid. Molecular weight of the synovial fluid in the range 500 to 1600 kD. 13C NMR spectroscopy may be available method to study the clinical biophysical changes in synovial fluid.

There is a vast number of metabolites detected in aqueous humor and vitreous humor examination with the help of NMR spectroscopy. These metabolites include acetate, acetoacetate, alanine ascorbate, citrate, creatine, formate, glucose, glutamine or glutamate, β-hydroxybutyrate, lactate, threonine and valine. 1H and 19F NMR spectroscopy have been applied to study the penetration of dexamethasone phosphate into the aqueous humour.

1H NMR spectroscopy of human saliva has been used in a forensic science. It has been established that parotid gland and saliva provide a well resolved 1H NMR spectrum, which shows significant circadian effects. 1H NMR spectroscopy has been used to study pancreatic juice and small bowl secretions. Several studies with proton magnetic resonance of the fluid from the cyst of kidney of patients with autosomal dominant polycystic kidney disease have been reported. The nuclear magnetic resonance spectra revealed a number of features and showed the cyst fluids to be distinct from both urine and blood plasma. The biochemical composition of the cyst fluids was attributed to abnormal transport processes occurring across the cyst epithelial wall.

It has been established in the literature that several studies have applied NMR spectroscopy to determine the number and identity of drug metabolites in bile. 2H NMR has been extensively employed to study the pharmacokinetics of benzoic acid in relation to function of liver.

Wüthrich, K. [10] has been written in his Nobel lecture article that the spectrum of a globular protein is more complex than the sum of the NMR lines from the constituent amino acid residues in the polypeptide chain. It has also been noted that the differences between the 1H NMR spectra of folded and unfolded forms of a polypeptide chain explained by different interactions with the solvent. NMR is capable of providing structural informations on partially folded polypeptides. The ability of NMR spectroscopy to give a best picture of macromolecular structures and their intermolecular interactions with high spatial and temporal resolution is a demand of research. It has been seen that supplementing the determination of protein folds with data on intermolecular interactions provides a key for the identification of unknown gene functions also. The 1H atom is the only atom normally present in proteins and can be observed by NMR. All the 1H atoms may be observed, except these labile hydrogen atoms of − NH−, − NH2, −OH, and −SH groups that may exchange with hydrogen atoms in the aqueous solvent at fast speed. If pH is acidic the exchange of hydrogen with solvent is very slow. We can make the exchangeable hydrogen atoms invisible by placing a protein sample in 2H2O. Each hydrogen

atom in a protein can be resolved by NMR of unique chemical shift, which entirely depends on the bonded atom with its environment.

The chemical shift of a nucleus is dependent on the electron density around the nucleus. The electron density is directly dependent on the type of nucleus and on the number, nature and location of neighboring atoms. Chemical shift offer an important source of local structural information. Chemical shifts are dependent on a variety of other factors such as ring currents and hydrogen bonds. The author has supplied informations related to NMR studies of structure and function of biological macromolecule. NMR spectroscopy is unique among the techniques available in science for 3-dimentional structure determination of proteins and nucleic acids. NMR can be done in solution. Body fluids such as blood, stomach liquid and saliva and protein solutions where these molecules perform their physiological functions. Study of the molecular structures in solution is to much relevant and desirable. Solution conditions such as the temperature, pH and salt concentration can be adjusted so as to closely mimic a given fluid (physiological fluid). Solutions can be changed into non-physiological conditions such as protein denaturation. NMR investigates the dynamic features of the molecular structure, as well as studies of structural, thermodynamic and kinetic features of interactions between proteins other solution components. These may be other macromolecules or low molecular weight ligands.

Some of the major improvements in NMR hardware and methodology have been made by the scientists. Due to these improvements the use of NMR for the characterization of structure and dynamics of biological molecules in solution has become very important. These improvements are still into consideration and on going and are designed to overcome the main problem with NMR of biomolecules, namely signal to noise ratio and spectral overlap. Biomolecular NMR spectroscopy may give information about conformational dynamics and exchange processes of biomolecule at time scales ranging from 10^{-8} seconds (picoseconds to seconds). This technique is also effective in determining ligand binding and mapping interaction surfaces of protein /ligand complexes.

Proteins are orders of magnitudes larger than the small organic molecule. NMR spectroscopy is applied to study of proteins because increased number of each element present in the molecule.

2. REVIEW OF LITERATURE

The application of NMR in the study of biological molecules has become an important ingredient. This technique was first applied to investigate the bulk material by Purcell, E.M. [11] and Bloch, F.et. al. [12]. Pioneering work was carried out by Jardetzky , O. et.al . [13], Kowalsky ,A. et.al. [14] and Mc Donald ,C.E. et.al. [15] in the field of relevant biomolecules. Proteins are the most studied by biopolymers. The protein spectra are very complex and

simulation by mixing of amino acids does not produce the replica of the observed spectra in them as the intricate folding at the polypeptide chain makes major changes in both chemical shift as well as relaxation effect (line broadening).

Important structural information are revealed by NMR spectra, which are characterized by parameters like peak position, width, intensity and multiplicity of its line. One can find the different proton groups present in the molecule by the number of lines present in NMR of a particular molecule. The integrated area of a line gives the relative number of protons in each groups and also information about the environment of the molecule. The hyperfine splitting reveals the interaction between a particular nucleus and its neighbors. The line width increases with the size and rigidity of the molecule. However in a large molecule there is an overlapping of peaks which can be overcome by increasing the frequency of the spectrometer. The NMR spectra arise due to the absorption of energy during transition from low to the higher energy state in a nucleus. The detectable absorption is characteristics of the environment of the nucleus. With the variation of frequency the resonance will be the function of the local molecular environment and of the magnetic field in which the nucleus find itself.

Improvement in NMR technology is one of the most recent method, applied to the diagnosis of human diseases [16-19]. Chalovich, J.M. et.al.[17] have given a statement that the nuclei common in tissues   was used for NMR imaging of the organs of human subjects and to analysis the composition of human serum of the various applications of NMR for medical purpose, the method is most sensitive for analysis of serum. Bradbury, E.M. et.al. [20] has also applied NMR in the investigation of structure of histones Lee, A.G. et.al. [21] and Chapman, B. et.al.[22] have studied molecular basis of interaction of histones with nucleic acid, analysis of flexibility gradient in phospholipids membranes and in understanding the biological importance of bound water.

Kurosu, H. et al. [23] have studied synthetic macromolecules with the help of NMR. NMR has been the most suitable technique to characterize and to investigate the correlation between the structure and physical properties. Prior, M. J. W. [24] has studied NMR in living systems such as eye, tissue of heart muscle, reproductive tissue, brain, liver, bone marrow, etc. The author has reported that the linewidth of lipid and water differed significantly between groups.

Jardetzky, O. [25] has reported the finding on determination of macronuclear structure and dynamics by using NMR. He pointed out the basic problem of interpreting spectroscopic data in structural terms from the fact that measured parameters represent motional as well as ensemble averages. If we have a non-rigid system, a unique correlation between measured spectroscopic parameters and structural parameters such as interatomic distances and coordinates does not exist. A straightforward calculation of the structure is not possible.

NMR parameters are the function of distances, motions, frequencies and amplitudes. These parameters can supply the well defined relationship regarding the interatomic distances.

Hounsell, E. [26] has studied carbohydrates, lipids and membranes with the help of NMR. There is a study on cerebrospinal fluid of different diseases and a clear cut differentiation was found in the atomic and molecular level in terms of chemical shifts.

Simpson, P. J. [27] has studied and reported the findings on proteins and nucleic acids. The assignment of small proteins is regular system nowadays. The specific amino acid labeling can still be of use for assisting peak identification.

Consanni, R. et al. [28] have studied nuclear magnetic resonance and chemometrics to access geographic origin and quality of traditional food products. They have reported their view for NMR and chemometrics, which were reviewed and applied to food quality and geographical origin determination.

Adam, A. et al. [29] have applied carbon-13 NMR to study the proteins and glycoproteins. They have also studied globular proteins and recorded NMR spectra at 15.18 MHz. Some overlap between the aliphatic region and amino acid residues has been obtained. NMR can be used as a tool to study the bio-molecules in the field of biochemistry. Talebpour, Z. et al. [30] have applied this technique to identify and determine the caffeine and theophylline in human serum. They have reported their findings for the caffeine peaks which were obtained at 2.75, 2.93 and 3.40 ppm. Theophylline peaks were found at 2.77 and 2.97 ppm.

Wishrat, D. [31] has studied NMR technique for the determination of proteins with the development of drug discovery. It has been noticed that the first crude protein structure was determined in the year 1980. NMR can play a role in the area of protein based drug discovery. It gives the structural information along with the dynamics of the protein.

Alexander, L. et.al. [32] have given efficacy of proton magnetic resonance spectroscopy in neurological diagnosis and neuro therapeutic decision making . Anatomic and functional neuro imaging with magnetic resonance imaging (MRI) includes the technology more widely called magnetic resonance spectroscopy (MRS) . This technique assays regional neurochemical health and disease .It is the most accessible diagnostic tool for clinical management of neurometabolic disorders. Due to noninvasive nature of this spectroscopy it is an ideal tool for therapeutic monitoring of disease and neurotherapeutic decision making . The authors stated that this technique provides therapeutic impact in brain tumors , metabolic disorders such as adrenoleukodystrophy , Canvan's disease , Alzheimer's disease , hypoxia , secondary to trauma or ischemia , human immunodeficiency virus dementia and lesions , hepatic and renal failure . Magnetic   resonance spectroscopy defines neurochemistry on a regional basis by acquiring a radio – frequency signal with chemical shifts from one or many voxels or volumes . They have also reported that each neurometabolite is localized on a horizontal scale i.e.

chemical shift . The relative metabolic concentration of them is determined from metabolite's peak . Engelhardt , E. et. al. [33] have studied limbic regions with the help of nuclear magnetic resonance spectroscopy . Authors suggested that the results made possible the early diagnosis , to follow the degenerative process throughout the course and to suggest a spectroscopic staging related to the clinical stages of Alzheimer's disease. Soher, B.J. et.al. [34] have studied and reviewed 1H MR spectroscopy in Alzheimer's disease and demonstrated metabolic differences between patients who have Alzheimer's disease and cognitive normal age–matched controls . Clinical magnetic resonance spectroscopy also shows regional variations in metabolites between patients who have AD and those who have other dementias . Single – voxel and volumetric standard magnetic resonance spectroscopy techniques and automated data processing software are available for clinical MR scanners. Rhinehart , D.L.et.al .[35] have applied MR spectroscopy to Alzheimer's disease . They have stated that this spectroscopy is a technique that permits noninvasive evaluation of biological metabolites .We can measure metabolites associated with Alzheimer's disease. Scientists are trying to find a distinct connection between the disease and certain metabolites so that an accurate diagnosis can be made during a patients' life. Westman, E.et.al. [36] have studied magnetic resonance imaging and magnetic resonance spectroscopy for early detection in Alzheimer's disease. Authors have investigated whether the discrimination between early Alzheimer's disease and elderly healthy control subjects can be improved by adding magnetic resonance spectroscopy measures to magnetic resonance imaging (MRI) measures. The method of their study showed strong potential for discrimination between Alzheimer's disease and controls. Azevedo, D. et.al. [37] have studied proton spectroscopy in Alzheimer's disease and cognitive impairment no dementia . They have confirmed on the basis of proton magnetic resonance spectroscopy the hypothesis metabolic alterations are present . Combining magnetic resonance spectroscopy from different cerebral regions can help in the diagnosis . Frederick, B.D.et.al. [38] have studied changes in brain after treatment of Xanomeline with the help of magnetic resonance spectroscopy . They have shown a positive correlation between changes from baseline in parietal lobe grey matter cytosolic choline, expressed in terms of choline /creatine resonance ratios, and cognitive performance as measured with the Alzheimer's disease assesment scale cognitive subscale . They have also found increased levels of cystolic choline , a precursor pool for acetylcholine synthesis associated with greater progression in memory impairment during treatment .

Jonathan, K. et. al. [39] have studied magnetic resonance spectroscopy in Alzheimer's disease . They have given a thought that this spectroscopy may provide a window into the biochemical changes associated with the loss of neuronal integrity and other neurodegenerative pathology, which involves the brain before the manifestation of cognitive impairment in patients at risk for Alzheimer's disease. Colla, M.et.al. [40] have used magnetic resonance spectroscopy in Alzheimer's disease . They have stated that the altered metabolite

signals and ratios in combination with the cognitive performance might suggest gender – related neuronal degeneration and dysfunction with subcortical regions in this disease. Chen, J.G. et.al.[41] have studied magnetic resonance spectroscopy in Alzheimer's disease with focus on N-acetylaspartate. They have reported significantly lower N-acetylaspartate levels in Alzheimer's disease brain than in control brains. Kantarci, K. et. al. [42] have studied 1H magnetic resonance spectroscopy in dementia and suggested that this spectroscopy may also be valuable in predicting future development of dementia and monitoring early disease progression for preventive therapies . The potential clinical application of this technique in aging and dementia is growing with technical advances in the field of research. Doraiswamy, P. M. et. al. [43] have studied magnetic resonance spectroscopy for prediction of cognitive decline in early Alzheimer's disease and suggested that the interest is developing in markers of neurodegeneration and have prognostic value even in earliest stages of Alzheimer's disease . The availability of such type of markers would facilitate the development of therapies to delay the onset or slow the progression of this disease .This technique enables the non-invasive in - vivo assessment of brain metabolites, such as N-acetylaspartate and myoinositol .Antuano, P. G. et. al. [44] have studied decreased glutamate in Alzheimer's disease, which was detected in vivo with the help of nuclear magnetic resonance spectroscopy at 0.5 Tesla and suggested that glutamate and glutamine reduction may be a biological marker for early clinical diagnosis of Alzheimer's disease. Chantel, S. et. al. [45] have studied proton magnetic resonance spectroscopy in mild Alzheimer's disease and given their findings, which were consistent with regional distribution of neuropathologic changes   and cognitive symptoms characterizing early phases of this disease and with the pattern of lateralization of normal brain function .

Kantarci, K. et. al. [46] have   studied 1H NMR spectroscopy in common dementias and found that ratio of levels of N-acetylaspartate and creatine were lowered in dementias, which were characterized by neuron loss, such as Alzheimer's disease, frontotemporal lobar degeneration and vascular dementia. The ratio of levels of   myoinositol and creatine were elevated in dementias that are pathologically characterized by gliosos. Choline and creatine levels were higher in dementias, which were characterized by a profound cholinergic deficit such as Alzheimer's disease and dementia with Lewy bodies. Huang, W. et. al. [47] have studied brain metabolic concentration and dementia severity in Alzheimer's disease. They have shown that the measurements with proton magnetic resonance spectroscopy of absolute metabolic concentration in the neocortex showed abnormal concentrations of brain metabolites in Alzheimer's disease. Concentrations of these metabolite do not occur with disease severity. The changes in myo–inositol and creatine occur in the early stage of Alzheimer's disease.   N-acetylasparatate abnormality does occur in mild Alzheimer's disease but progressively change with dementia severity. A differentiation between controls and Alzheimer's disease can be made with the help of proton magnetic resonance spectroscopy. Shino, A. et. al. [48] have studied proton magnetic resonance spectroscopy with

dementia and shown that there are three peaks corresponding to N-acetylasparatate, creatine with phosphocreatine and choline containing compounds. The ratio of N-acetylasparatate with creatine might reflect the number and activity of neuronal cells in brain. This technique may prove a useful tool for early detection of dementia and other neurological disorders. Shonk, T. K. et. al. [49] have studied probable Alzheimer's disease diagnosis with the help of magnetic resonance spectroscopy. They have found that a reduction in levels of N- acetylasparatate and and increase in levels of myo-inositol characterize Alzheimer's disease. They have also concluded that this technique enabled identification of mild to moderate Alzheimer's disease with a specificity and sensitivity of clinical utility. Alexandra, J. S. et. al. [50] have studied NMR spectroscopy to study CSF and serum in neurological disorders. They have shown that NMR spectroscopic metabolic profiling of CSF and serum can identify differences between neurological disorders .Tukiainen,T. et. al. [51] have studied a multi metabolic analysis of serum by 1H NMR spectroscopy for early systemic signs in Alzheimer's disease. They have suggested that the application in cognitive impairment gives a distinct role of systemic lipid metabolism, particularly the metabolic syndrome and the relative amount of srum   fatty acids, in the risk of assessment in Alzheimer's disease. Authors have also estimated the levels of glycoproteins, which were elevated and may be a cause of risk factor in Alzheimer's disease. Ghauri, F. Y. K. et. al. [52] have studied human post mortem cerebrospinal fluid in Alzheimer's disease with the help of nuclear magnetic resonance spectroscopy. They have concluded on the basis of measured levels of citrate and disease state that these levels were significant. The citrate level may be used as a marker. Bell, J. D. et. al. [53] have studied body fluids with the help of this technique. Authors have used urine, sweat, aqueous humor, amniotic fluid, seminal plasma, cerebrospinal fluid, synovial fluid and blood plasma and concluded that urine has low content of protein. Blood plasma contains high protein content. On the basis of their findings it is possible to detect not only small molecules but also mobile regions of macromolecules and to demonstrate the interaction of anions such as lactate with proteins.

3. MATERIALS AND METHODS

The blood samples of Alzheimer's disease patients and controls were collected from the Department of Neurology, Safdarjang Hospital, New Delhi. Twenty milliliters freshly drawn blood from each patient was collected in clean and dry test tube without any anti-coagulant. The test tube was kept for 45 minutes at room temperature $(22 \pm 2\,^{0}\text{C})$ for the formation of clot. Sera of different patients were separated by centrifugation at 1500 r.p.m. upto 15 minutes and were collected in screw capped test tubes.

IgG sample were prepared on protein A –Sepharose [54].

The IgG binding properties of protein A, make affinity chromatography with protein A--sepharose CL- 4B a very simple method for preparing IgG. 1.5 g protein -A sepharose CL-4B was swollen in 10 ml phosphate buffered saline (PBS) for 1 hour at room temperature and then

packed into a small chromatography column. 10 ml human serum was diluted with an equal volume of PBS. The serum was filtered through the column at a flow rate of 30 ml/h. Washing was done through unbound protein with PBS. Until no more protein left the column (the protein was monitored with a UV flow cell).

The bound IgG was eluted with glycine-HCL buffer having a pH value of 2.8. The pH of the purified IgG solution was titrated to near neutrality with NaOH and dialysed against PBS. The column was regenerated by washing with 2 column bed volume of PBS. The column was stored at 4°C.

The protein A content of the swollen gel is 2 mg/ml and the binding capacity for human IgG is approximately 25 mg/ml of packed gel. As the binding of protein A to IgG involves tyrosine residues on the protein A glycosyl tyrosine (0.1M in 2 % (NaCl) can be used to elude the IgG rather than the the glysine –HCl buffer.

The NMR spectra of the IgG samples extracted from normal person and epileptic patients were recorded on Av Bruker 500 MHz NMR Spectrophotometer (Fig. 3) in central NMR facilities I.I.T. New Delhi, India.
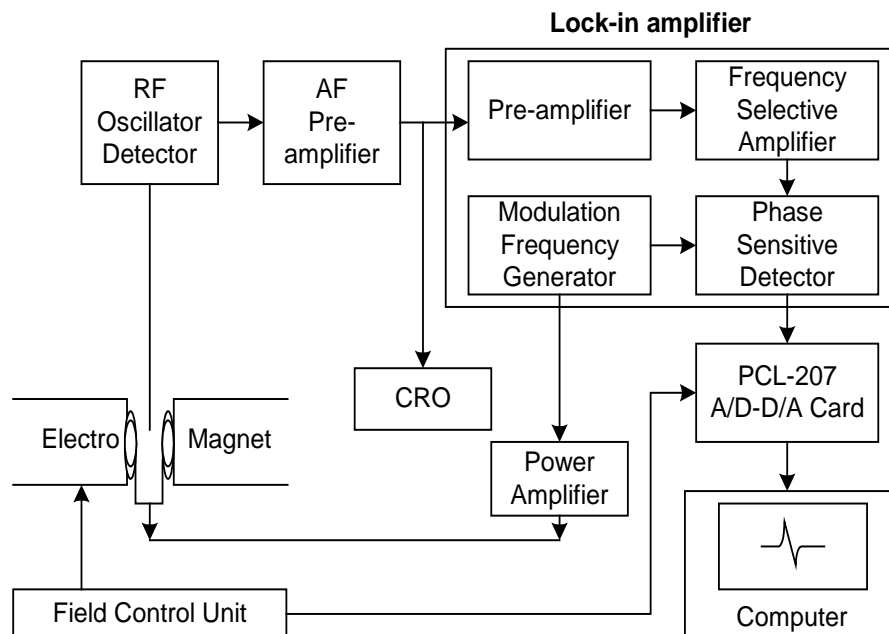

Fig. 4 Block diagram of Nuclear Magnetic Resonance Spectrometer

4. RESULTS

We have applied NMR spectroscopy to IgG molecule of Alzheimer's disease and findings are reported in the table form. We have compared our data with the normal healthy controls. Typical NMR spectra of normal and Alzheimer's disease patient are given in Fig.5 to Fig. 19.
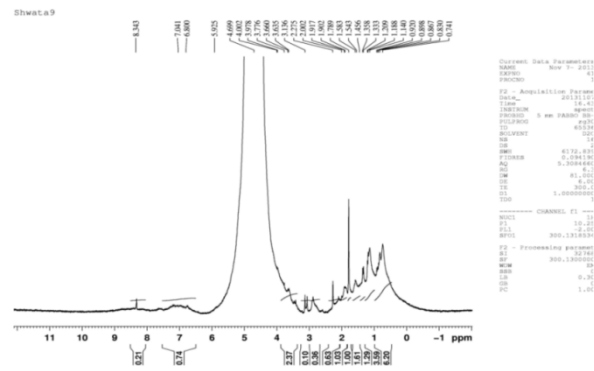
Fig.5 . Typical NMR spectra of normal sample

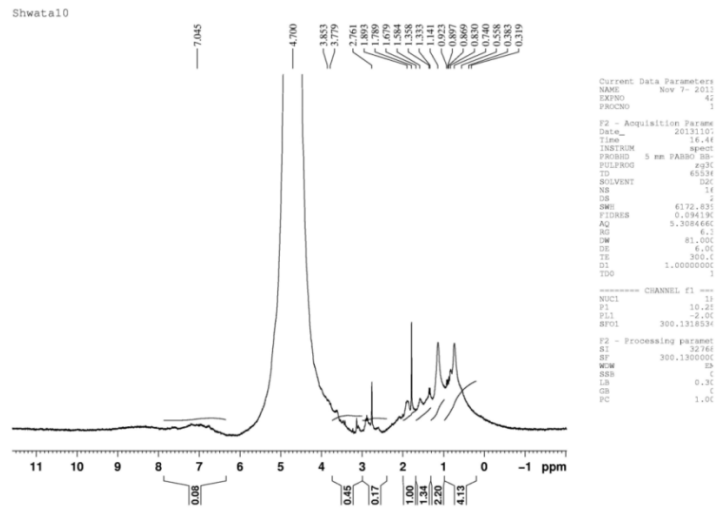**Fig.6 . Typical NMR spectra of normal sample**
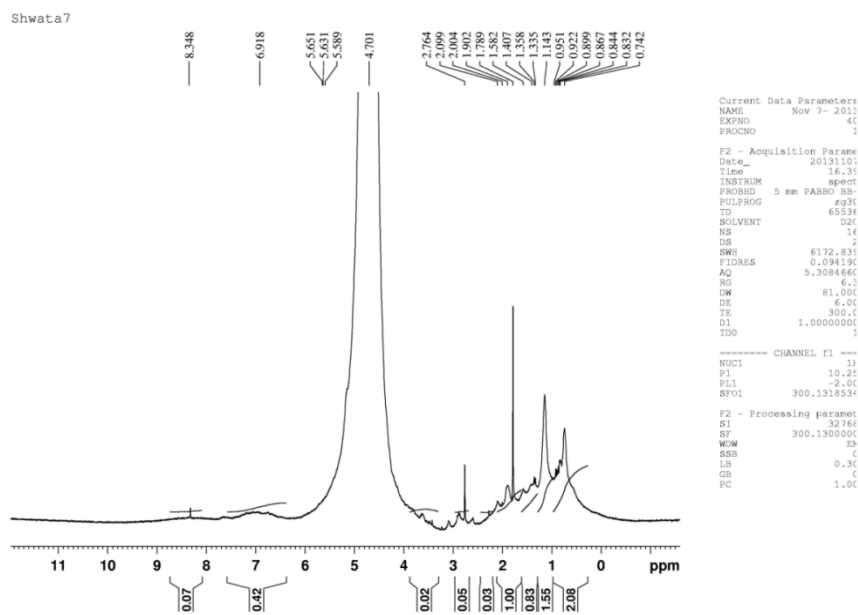
Fig.7 . Typical NMR spectra of normal sample

Fig.8 . Typical NMR spectra of normal sample

Fig.9. Typical NMR spectra of normal sample

Fig. 10. Typical NMR spectra of AD sample

Fig. 11. Typical NMR spectra of AD sample

Fig. 12. Typical NMR spectra of AD sample

Fig. 13. Typical NMR spectra of AD sample

Fig. 14. Typical NMR spectra of AD sample
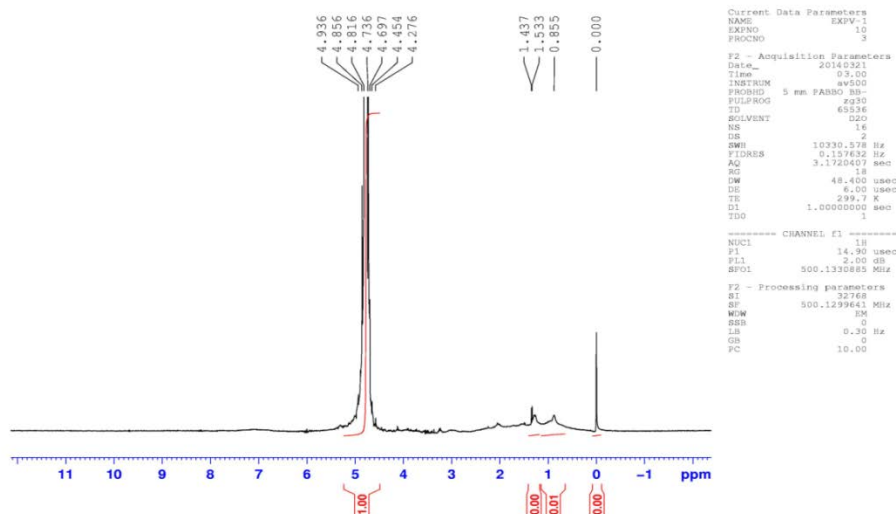
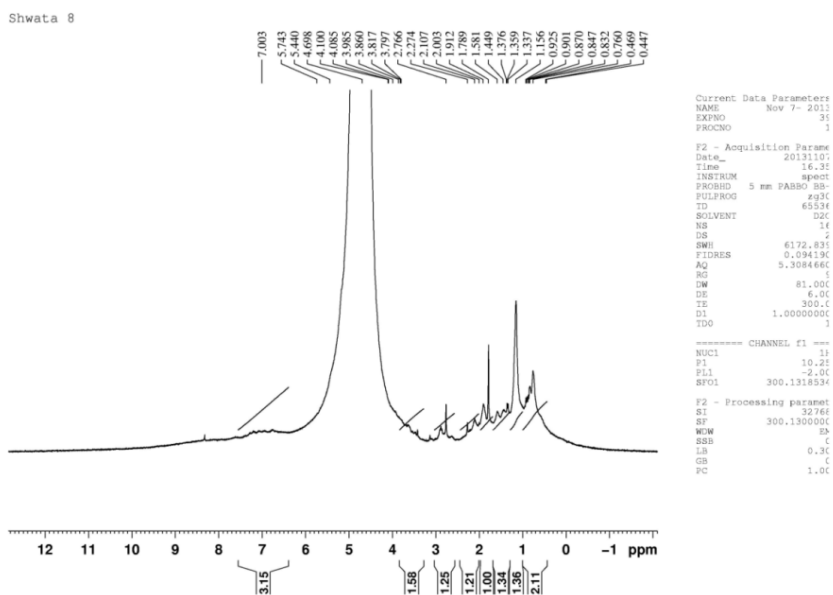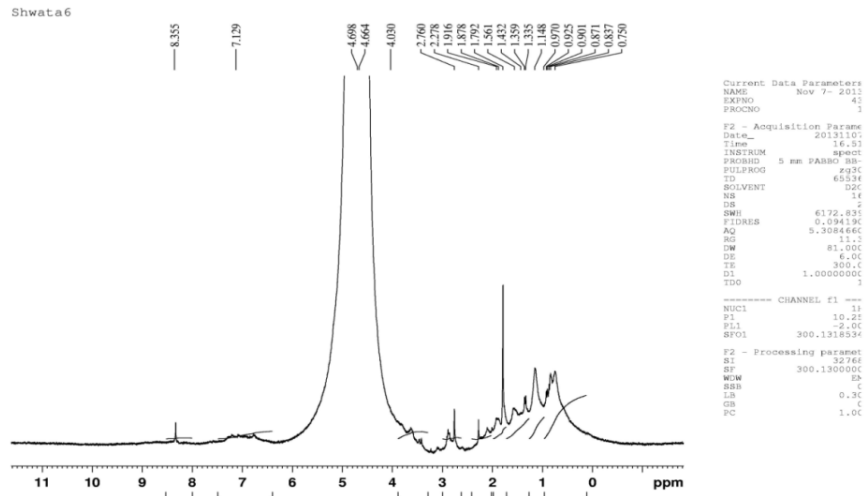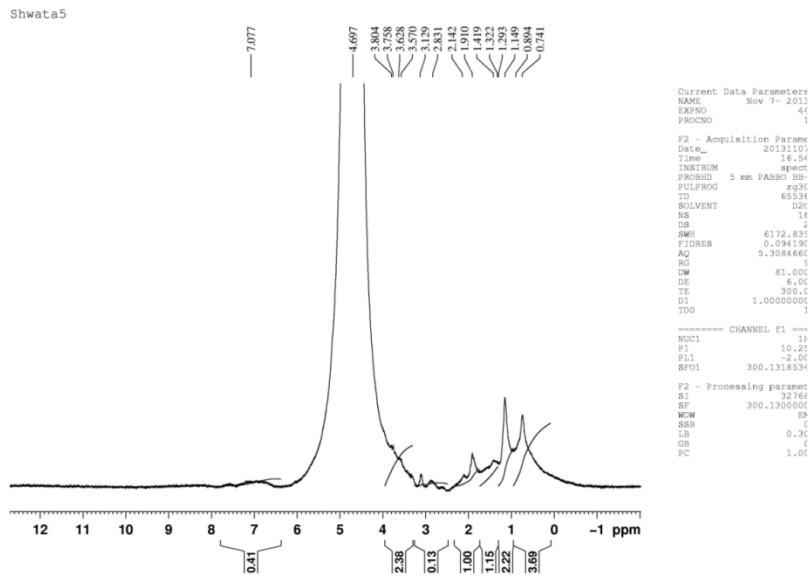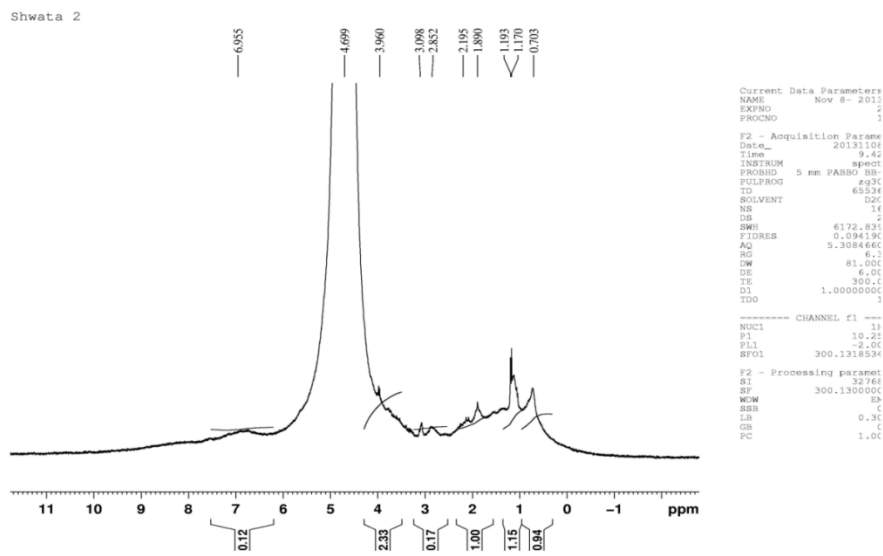**Fig. 15. Typical NMR spectra of AD sample**
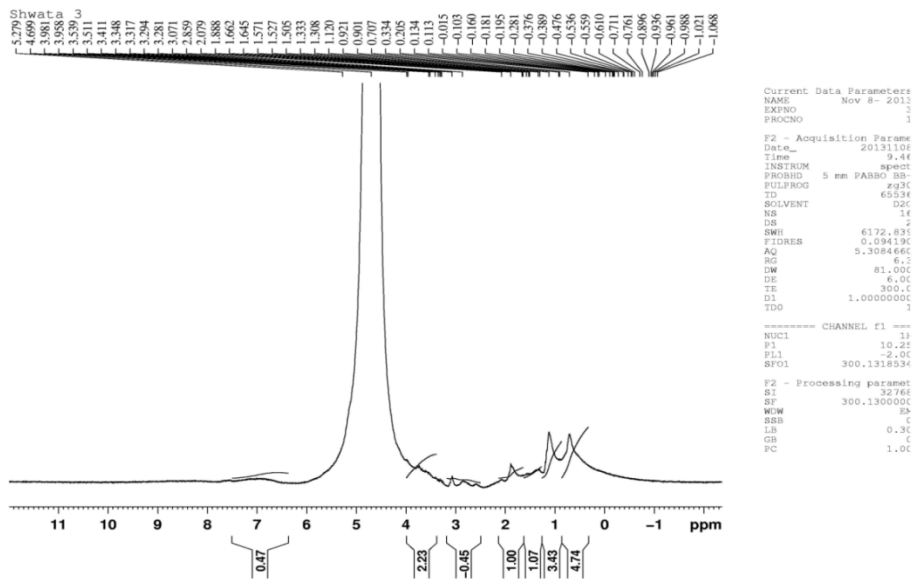

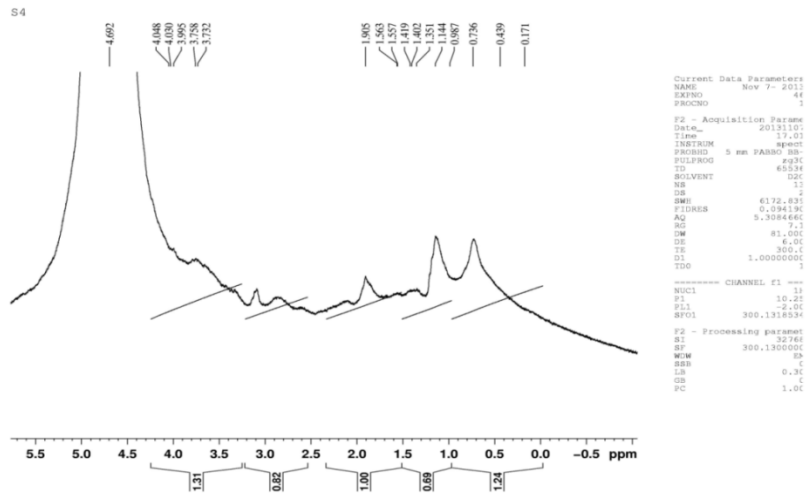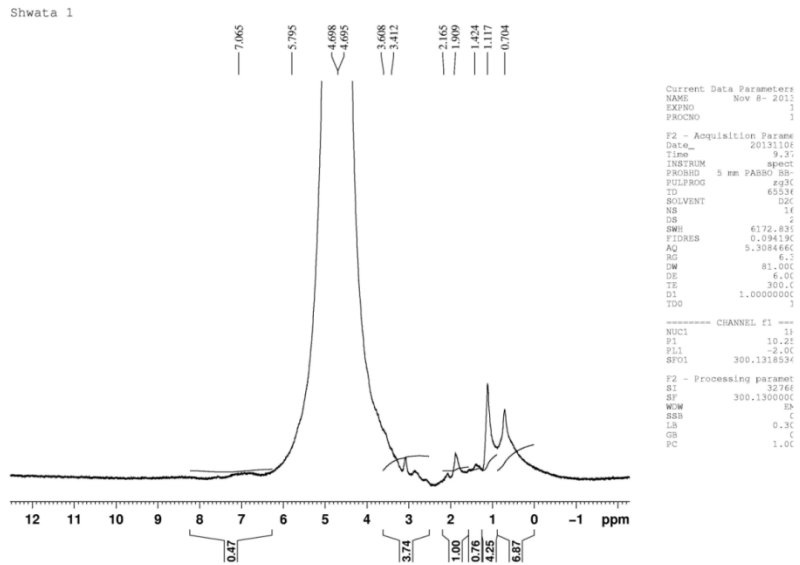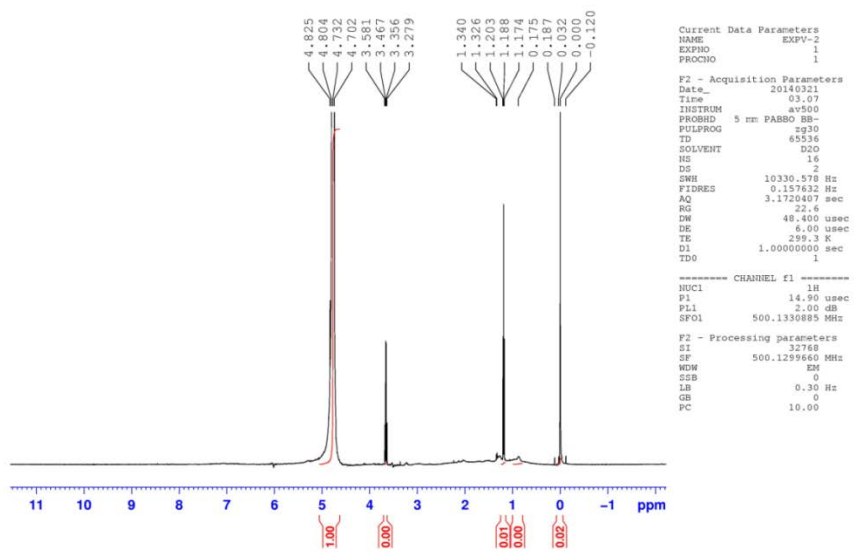**Fig. 16. Typical NMR spectra of AD sample**
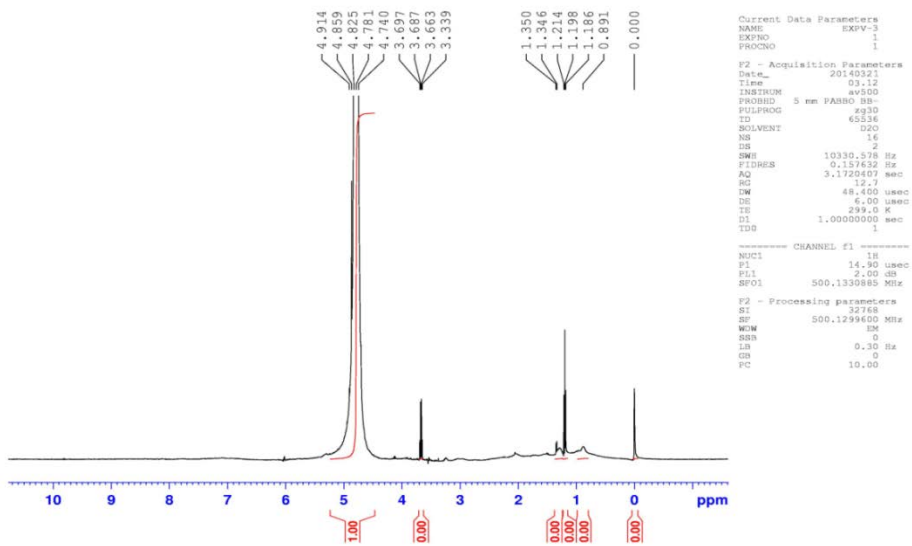
Fig. 17. Typical NMR spectra of AD sample
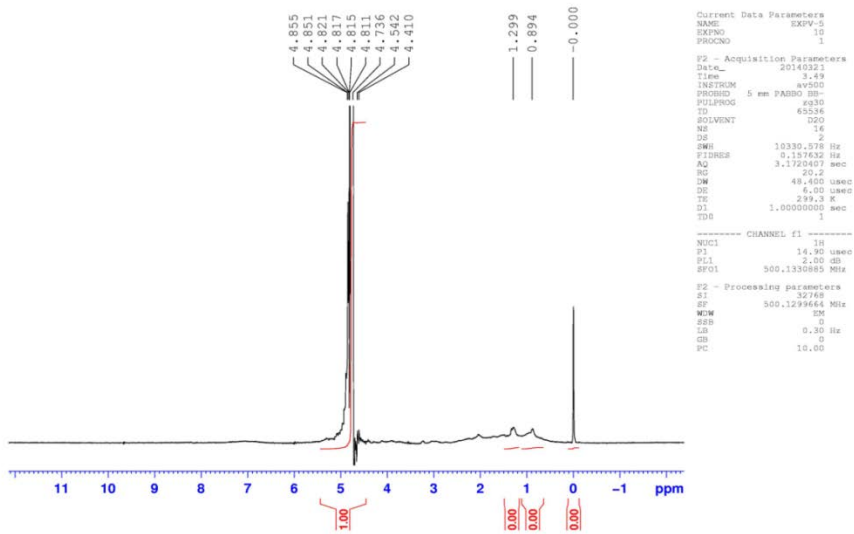
Fig. 18. Typical NMR spectra of AD sample
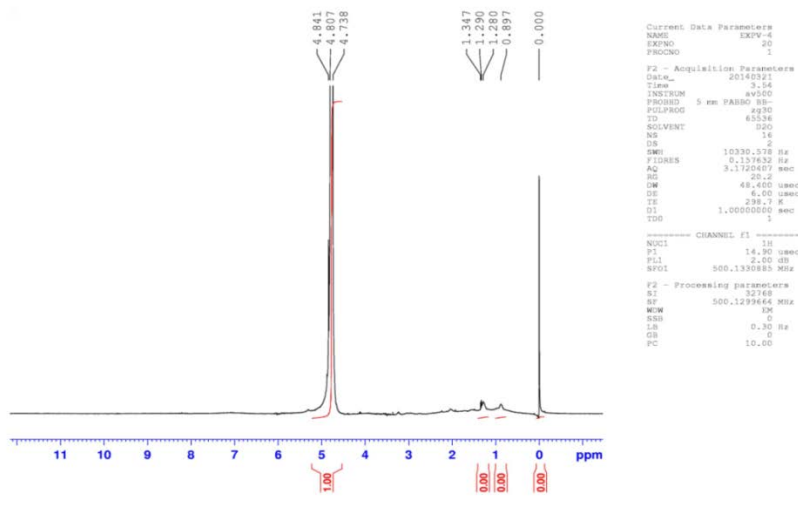
Fig. 19. Typical NMR spectra of AD sample

Table 2. Comparison between different probable groups of the amino acids of IgG with peak intensities in AD and Controls

S. No.	Type of sample	Peak position	Chemical shift δ pm	Probable group	Standard values	D_2O peak
1	N	1 2 3 4 5	0.62 1.00 1.70 1.82 3.62	Isoleucine(δ-CH$_3$) Isoleucine($\gamma-CH_3$) Leucine(β-CH) Proline(β-CH) Glycine(α-CH)	0.67 0.95 1.75 1.84 3.64	4.70
2	N	1 2 3 4	0.83 1.00 1.55 2.08	Isoleucine (δ-CH$_3$) Isoleucine($\gamma-CH_3$) Leucine(β-CH) Glutamic acid(β-CH)	0.89 0.95 1.65 2.09	4.70
3	N	1 2 3 4 5 6 7 8	1.00 1.21 1.25 1.34 1.36 1.58 2.11 3.15	Isoleucine(γ-CH$_3$) Isoleucine((γ-CH$_2$) Isoleucine(γ-CH$_2$) Alanine(β-CH) Alanine(β-CH) Leucine($\gamma-CH$) Phenylalanine(β-CH)	0.95 1.22 1.22 1.36 1.36 1.54 2.11 3.22	4.70
4	N	1 2 3 4 5 6 7	0.74 1.03 1.29 1.61 2.37 3.51 6.20	Isoleucine(γ-CH$_2$) -- Isoleucine(γ-CH$_2$) Leucine(β-CH) Glycine (γ-CH$_2$) Proline(δ-CH$_2$ ---	0.77 -- 1.48 1.65 2.35 3.46 ---	4.70

5	N	1 2 3 4 5	0.45 1.00 1.34 2.20 4.13	Isoleucine($\gamma - CH_3$) Alanine (β-CH) Proline(β-CH) ------ ----	0.95 1.36 2.21 ----- ---	4.70
6	AD	1 2 3 4 5	0.76 1.00 3.74 4.25 6.87	Isoleucine($\gamma - CH_3$) Isoleucine($\gamma - CH_3$) Serine $(\beta - CH_3)$ Glutamic acid $(\alpha - CH)$ Glutamic acid(NH_2)	0.77 0.95 3.79 4.22 6.87	4.70
7	AD	1 2 3 4	0.94 1.00 1.15 2.33	Isoleucine(γ-CH$_3$) Isoleucine(γ-CH$_3$) Isoleucine((γ-CH$_2$) Proline $(\beta - CH_3)$	0.95 0.95 1.16 2.28	4.70
8	AD	1 2 3 4 5	1.00 1.07 2.23 3.43 4.74	Isoleucine(γ-CH$_3$) Isoleucine(γ-CH$_2$) Proline $(\beta - CH_3)$ Tryptophane (β-CH) Aspartic acid $(\alpha - CH)$	0.95 1.16 2.21 3.41 4.76	
9	AD	1 2 3 4 5	0.69 0.82 1.00 1.24 1.31	Isoleucine(δ-CH$_3$) Isoleucine(δ-CH$_3$) Isoleucine(γ -CH$_3$) Isoleucine(γ-CH$_2$) Alanine(β-CH)	0.67 0.89 0.95 1.22 1.36	4.69
10	AD	1 2 3 4 5	1.00 1.15 2.22 2.38 3.69	Isoleucine(γ -CH$_3$) Isoleucine(γ-CH$_2$) Proline $(\beta - CH_3)$ Glycine(γ-CH$_2$) Serine $(\beta - CH_3)$	0.95 1.16 2.21 2.38 3.79	4.70
11	AD	1 2 3 4 5 6 7	0.855 1.43 1.53 4.27 4.45 4.69 ---	Isoleucine(δ-CH$_3$) Lysine(γ-CH$_2$) Leucine $(\gamma - CH_3)$ Glutamic acid (α-CH) Thr(α-CH) Cystine (α-CH) ----	0.89 1.45 1.54 4.29 4.50 4.69 -----	4.73

12	AD	1 2 3 4 5 6	1.17 1.32 3.27 3.46 3.58 ---	Isoleucine(γ-CH_2) Alanine(β-CH) Cystine(β-CH) Tryptophane (β-CH) Serine (β-CH) ---	1.19 1.36 3.28 3.41 3.79 -----	4.73
13	AD	1 2 3 4 5 6	0.89 1.18 1.35 3.68 4.74	Isoleucine(δ-CH_3) Isoleucine(γ-CH_2) Alanine (β-CH) Serine(β-CH) Aspartic acid(α-CH)	0.89 1.19 1.36 3.88 4.76	4.82
14	AD	1 2 3 4 5 6	0.89 1.29 4.41 4.54 4.73 ---	Isoleucine(δ-CH_3) Isoleucine(β-CH) Proline(α-CH) Serine (α-CH) Asp(α-CH) ----	0.89 1.36 4.41 4.52 4.76 ---	4.81
15	AD	1 2 3 4	0.89 1.28 1.34 4.73	Isoleucine(δ-CH_3) Isoleucine(β-CH) Alanine(β-CH) Aspartic acid (α-CH)	0.89 1.36 1.36 4.76	4.80

According to data available with the present study we are giving some of the findings related to AD patients. A group Aspartic acid (α-CH) is found in four cases only of AD patients and this group was absent in all the normal healthy persons. The group isoleucine (δ-CH_3) has been found in all the blood samples of normal persons and AD patients. Glutamic acid (α-CH) is found in two cases of AD patients and was absent in all the normal persons and other patients of AD. Alanine (β-CH) is found in two cases of normal healthy people and four cases of AD patients only. Asparatic acid (α-CH) is found in four cases of AD patients only and absent in all the normal healthy people. Lysine (γ-CH_2) is found in one case of AD patient only and absent in all the normal healthy controls along AD patients. Isoleuicine ($\gamma-$ CH_3) has been found in three cases of AD patients only and four normal healthy people. Cystine (α-CH) and Cystine (β-CH) have been found in two cases of AD patients only and absent in all the normals with AD patients. Tryptophane (α-CH) is found in two sample of AD patient only and absent in all the cases of AD and normal healthy people .

5. DISCUSSION

We have performed NMR spectroscopy with immunoglobulin 'G' and found very interesting groups present in the AD samples and some of the groups were completely absent in normal samples . It has been seen that there is some difference of chemical shift in the positions of the actual peaks. The shifting of chemical shift is a major point of discussion at this

stage. Chemical shifts are perhaps the most accessible and easily measured quantities in NMR spectroscopy. Chemical shifts for proteins reveals exquisitely detailed informations about backbone dihedral angles, side chain χ angles, hydrogen bond interactions, local electric fields, proximity and orientation of aromatic rings, ionization states, oxidation states, back bone dynamics, ring flip rates and even internuclear O-H distances. Chemical shift can play a useful role in delineating structural elements and even in refining and or defining the proteins tertiary structure. The most important application of chemical shift in biomolecular NMR is in the area of secondary structure identification and quantification. Protein chemical shifts may be used in structural analysis including secondary structure mapping, generating structural constraints, three dimensional structure refinements and three dimensional structure generations.

A magnificent use of NMR lies in fact that, because of the chemical shift, amino acids can be identified and isolated in the spectra of protein. It is well known in NMR theory that the motion of any type such as rotatory and translatory reduces the width of the resonance line. Due to this property motional narrowing feature starts and high resolution NMR is required. Proton magnetic resonance spectra of twenty amino acids and some representative di and tri peptide were studied by Mandel, M. [55].

Vitolis, C. et. al. [56] have studied NMR spectrum of a serum sample shows both sharp narrow peaks from small molecule metabolites and broad peaks from proteins and lipids. The analysis of spectrum of NMR for blood serum requires dealing with the effects of proteins and other large molecules.

NMR spectroscopy is the technique of spectroscopy that can provide detailed structural information about macromolecules at atomic resolution. Many scientists have been characterized small molecules by using empirical rules associated with the study of chemical shift regarding the conformation of the structure of the molecule.

It has been seen that most of the amino acid spectra can be understood on the basis of first order effects. The chemical shift is larger than the spin–spin coupling. In the study of amino acids while the chemical shift is not large compared to the spin–spin coupling. We can compare the chemical shift and spin –spin interaction in this situation. If we have a situation that lies between these two experiments there are many amino acids the spectrum may have first and second order both.

If we apply a large field to the system and we find a situation for the chemical shift, which is proportional to the field strength and kept spin –spin coupling as constant. Calculations based on chemical shifts are very useful in the structure of determination of globular proteins such as IgG.

Burton, D. R. [57] has studied the structure and function of immunoglobulin G and reported some of the interesting applications of NMR to study this molecule. An antibody is a

protein synthesized by an organism in response to invasion of the organism by a foreign substance termed as antigen. We have found principal antibody in serum as immunoglobulin G (IgG). IgG has a molecular weight of about 150,000 and a domain structure is shown in Fig. 20.
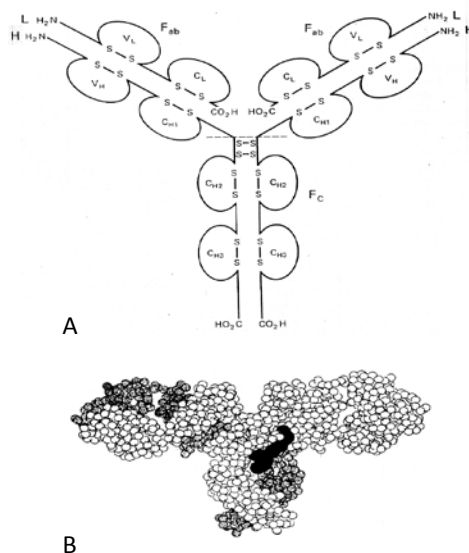

Fig.20. Schematic diagram of a typical Immonoglobulin (G) structure (A) and a space-filling model determined crystallographicaliy (B).

Mayer, M. et. al. [58] showed that IgG molecule can be cleaved into a number of proteolytic fragments. Antigen and complement bindings sites are also shown. If the antigen is not present, the complement site can be neglected. However, on the formation of a particular specifies antigen-antibody complexes, the first protein of the complement sequences binds to this site. This leads to activation of other proteins in the sequence and eventual destruction of the antigen.

It has been reported in the literature that IgG possess two equivalent tight Gd(III) sites located in the CH_3 domains of the Fc-region. Very much low affinity Gd(III) sites were also found on the FaS region. Experimental conditions may be adjusted such that IgG and the fragment Fc and pFc effects from the same two Gd(III) sites. They form a family of Gd(III) tight binding macromolecules of decreasing molecular weight. IgG has 150,000, Fc has 50,000 and pFc' has 25,000. There is an internal motion found in the Fc portion of IgG. A considerable amount of motional freedom at Fc position was also found. A flexible rigid transition in the IgG molecule as the trigger for complement activation was also pointed out by Huber et al. [59]. Boyd, J. et. al. [60] have studied the mobility of protein on the basis of high resolution protein NMR of Fc and pFc' fragments. The spectra of such fragments appear resolved compared to the spectra of other proteins of similar molecular weight.

Cohn, J. S. et. al. [61] have studied the observations of amino acid side chains in proteins using this sophisticated technique of spectroscopy and reported in the research article

regarding the side chain groups such as Glu, Asp, Lys, Arg, Met, Thr, Leu and others act as intrinsic non-disturbing probes of their local electronic microenvironment in a protein.

Some of the authors [62-64] have studied the structure of proteins with the help of NMR spectroscopy in detail. They have found each proton resonance appears along the chemical shift axis in the expected fashion. The multiplets due to spin coupling appear only on the perpendicular axis. If an amino acid residue in a protein is converted from a solvated state in a random coil polypeptide chain to buried inside the interior of a globular protein the chemical shift depends on the variation of magnetic susceptibility. Glick, R. E. et al. [65] have made their statements on amino acid residues and provide an interesting result such as chemical shift is directly proportional to the volume diamagnetic susceptibility K.

The NMR spectra of small globular proteins are very crowdy in nature. There is no evidence of unequivocal observations of Ser β-methylene proton resonance. Moore,R. et al. [66] have studied and found that the assignments of the methyl-group resonance of Thr-47 and Thr-89 for ferricytochrome C and ferrocytochrome C.

Some of the authors Spero, S. et. al. [67] and Kuszewski, J.Q.et.al. [68] have used chemical shift to obtain structural information regarding the correlation between chemical shifts and backbone torsion angles. It has been pointed out that different structures of proteins such as secondary, tertiary and quaternary have been successfully studied in solution and solid form and calculated with the help of chemical shift by various research scientists [69-76]. NMR chemical shifts are the best parameters and can be used in the structure elucidation of larger molecules. The assignment of backbone chemical shifts is necessary to determine the structure of protein.

Satoshi, E. et al. [77] have studied proton nuclear magnetic resonance of human immunoglobulin G1 and its fragments. They have pointed out some information regarding the structure of hinge region and effects of a hinge region deletion on internal flexibility.

Koichi, K. et al. [78] have studied structural basis of the interaction between IgG and fcγ receptors1. The studies on NMR spectroscopy show that Fcγ RII binds to a negatively charged area of the CH_2 domain, corresponding to the lower hinge region. The binding of Fcγ RIII onto one of the two related sites on the Fc induces a conformational change in the outer side.

Brab, A. W. et al. [79] have studied NMR analysis on immunoglobulin G and glycenes and they have provided their fruitful results as glycan does not directly engage the cell surface receptors. The termini of both glycan brachs are highly dynamic and experience considerable motion in addition to tumbling of the Fc molecule.

The three dimensional structure of globular protein fluctuates incessantly and the fluctuation is closely related to the function of the protein. Nicholson, L.K. et al. [80] have studied the dynamics of methyl groups in proteins.

Szilagyi, L. et al. [81] have identified a correlation between αH chemical shifts and the helical and β-sheet structures. If the other effects are not present, helical conformation produces up field shifts while β-structures shift the α proton downfield. Pasture, A. et al. [82] have studied the secondary structure of proteins and Oldfield, E. [83] studied three dimensional structure of proteins in terms of chemical shifts.

Jardetzky, O. et. al. [84] have studied the protein spectra of amino acids and indicated these chemical shift are independent of concentration. Chemical shift mean a change in the chemical shift from that of the free amino acid. The real use high resolution NMR lies in the fact that because of the chemical shift specifies amino acids, which can be nicely and easily isolated in the spectra of protein. If we increase our understanding of the relationship between the chemical shifts and structure of the proteins or globular proteins such as immunoglobulin G molecule, we will be able to improve the accuracy of measurement and structure determination.

Proteins play a major role in the billions of process which occur in the body. It includes the development of muscles, skin, digestion of food, growth of cells and the germination of human emotions. These cells have a tendency to produce proteins continuously. We are not able to understand how these complex molecules exactly work.

Not only is the chemical composition of the proteins but also the spatial structure of proteins important for the performance of their functions. The way in which they fold and unfold in 3-D space help in determining the function of the molecules.

It will be very difficult to understand the function of the molecules without detailed knowledge about their structure, spatial structure study is necessary now a day. NMR may help in the study of the determination of the structure of proteins. This technique can detect and quantify folding and conformation changes in proteins, while simultaneously providing detail structure information. If we use NMR spectroscopy in different diseases the NMR spectral peak observations can support the reliability of clinical applications. These peaks can determine the biochemical cause of the disease. Chandra, R. K. [85] has written somewhere else in literature that the interaction between nutrition and immunity focused on protein–energy malnutrition. The absorption, transfer, and distribution of many trace elements are not independent on specific binding and transport of proteins. Thus it is not surprising that changes in the concentration of trace elements exert large impact on immune responses. The process of inflammations increases vascular permeability and allows anti body, complement and other proteins to pass out the circulation and enter the extravaseular space. It may also induce inflammatory cells including lymphocytes to cross the vascular endothelium and accumulate in the tissues. Total net effect is to deploy all the resources of the immune system at the site of injury. Cells antibody and complement leave the blood and go into action where the demand is

high. It may be in the affected tissue outside the vessel wall .The effect is to abrogate in CNS, if only temporarily, its isolation from the immune processes of the body. The barrier, which excludes plasma proteins from the brain breaks down, allowing antibody to enter the extra vascular space. The amount of proteins in CSF increases and with it the level of immunoglobulin. Immunocompetent cells enter the CNS. The CNS now becomes capable to generating an immune response [86]. The appearance or disappearance of NMR groups may be changes in the CNS due to alteration in trace elements and immunity .Immunity is related with the trace elements suggested by Chandra, R. K. [85]. However , peak identification ,peak intensities ,peak analysis of the given sample is a big support for the research scientists and clinicians. Our study is a step for best approach in the field of spectroscopy .Further more detailed study is still required in this area .

6. CONCLUSION

The observed chemical shift in water peak in all the cases may be due to pathological conditions. There is overlapping of protons from the changed line width. We have found peaks in all the spectra recorded on NMR due to the formation of some active centre's such as paramagnetic ions. The comparison of the diseased sample spectra with the normal's reveal some characteristics of the disease. The group isoleucine (δ-CH$_3$) has been found in all the blood samples of normal persons and AD patients. Tryptophane (α-CH) is found in two sample of AD patient only and absent in all the cases of AD and normal healthy people .

It is possible to identify the nature of the pathological disorder by looking at the NMR spectrum of patient's blood (immunoglobulin G molecule). It has been found that the peak intensities, line shapes and chemical shift were different. These basic properties suggest that there are perturbations present, which vary from sample to sample. These perturbations are due to the presence of some unpaired electrons. The chemical shift suggests a transfer of electrons in enzymes and proteins in AD samples. The dipolar anisotropy of unpaired electron causes a shift in line position. Sometimes delocalization is also coupled. The appearance and disappearance of groups is a major contribution of the present work. Our earlier work on different types of spectroscopy such as ultraviolet, Fourier transform spectroscopy, atomic absorption spectroscopy supporting the data in this disease.

IgG.Authors are thankful to Mr.Deepak Singh, Central NMR facilities, I.I.T Roorkee for conducting experimental work.

REFERENCES

1. Jacobson, B., W. A. Anderson and J. T. Arnold, *A proton magnetic resonance study of hydration of deoxyribonuclease acid*, Nature,Vol. 173, 1954 : pp.772-773.

2. Saunders, M., A. Wishnia and J. G. Kirkwood, *The nuclear magnetic resonance spectrum of ribonuclease*, J. Am. Chem. Soc. Vol. 79, 1957 : pp.3289-3290.

3. Dwek, R. A., Nuclear *magnetic resonance (NMR) in Biochemistry, In : Applications to enzyme systems.* Oxford, Clarendon Press, I. S. B. N.0-19854614-9, 1973 : pp. 474.

4. James, T. L., *Nuclear magnetic resonance in biochemistry, In : Principles and applications, Academic Press,* New York, 1975 : pp. 46-11,177-181.

5. Wuthrich, K., *NMR in biological research, In : Peptides and proteins, American Elsevier*, New York, 1976 : pp. 379.

6. Jrrdetsky, O. and G. C. K. Roberts, *NMR in molecular biology, Academic press,* New York, 1981 : pp. 63-65.

7. Bloch, F., *Nuclear induction*, Phys. Rev., Vol. 70, No. 7-8, 1946 : pp.460-474.

8. Phillips, W. D., *Nuclear magnetic resonance spectroscopy of proteins. In : Enzyme structure. Edited by Hirs, C. H. W. and Timasheff, S. N., Methods of Enzymology*, Vol. XXVII, No. Part D, 1973 : pp. 825-890.

9. Lindon, J. C. and J. K. Nicholson, *Biofluids studied by NMR, In : Encyclopedia of spectroscopy and spectrometry, Edited by Tranter, G. E. and Holmes, J. L*. Academic press, London, 2000 : pp98-116.

10. Wuthrich, K., *NMR studies of structure and function of biological macromolecules,* Noble lecture*, 8, Dec., pp. 2002 : 235-267.

11. Bloch, F., W. W. Hansen and M. PackKard, *The Nuclear induction Experiment*, Physical Review*, Vol.* 70, No. 7-8, 1946 : pp.474-485.

11. Purcell, E. M., *Resonance absorption by nuclear magnetic moment in a solid*, Physical Review, Vol. 69, 1946: pp. 37.

13. Jardetzky, O. and N. G. Jardetzky, *Application of Nuclear Magnetic resonance spectroscopy to study of macromolecules,* Ann. Rev. Biochem., Vol.40, 1971 : pp. 605 -674.

14. Kowalsky, A. and N. Cohn, *Applications of Nuclear Magnetic Resonance in biochemistry*, Ann. Rev. Biochem., Vol.33, 1964 : pp. 481-518.

15. McDonald, C. E. and W. D. Phillips, *Fine structure of proteins and nucleic acids (Biological macromolecule series 4), Edited by Fasman, G. D. and Tunasheff, Marcel Dekker*, 1970 : pp. 1.

16. Edward R. H. T., M. Joan Davvson, D. R. Wilkie, R. E. Gorden and D. Shaw, *Clinical use of nuclear magnetic resonance in the investigation of myopathy*, Lancet, 1982 : pp. 725.

17. Chalovich, J. M., C. T. Brut, M. J. Danon, T. Glonek and M. Barany, *Phosphodistress in muscular dystrophies,* Ann. N. Y. Acad. Scie.,Vol. 317, 1979 : pp. 649.

18. Chance, B., S. Eleff and Jr. J. S. Leigh, *Non-invasive, Nondestructive Approaches to Cell Bioenergetics,* Proc. Nat. Acad. Sci., USA, Vol. 77, 1980 : pp. 7430.

19. Misra , L. K., S. R. Kasturi, S. K. Kundu, Y. Harai, C. F. Haziewood, M. G. Luthra, W. S. Yamanashi, R. P. Munjal, S., R. Amety, *Evaluation of muscle degeneration in inherited muscular dystrophy by nuclear magnetic resonance techniques,* Magn. Reson. Imag., Vol. 1, No.2, 1982 : pp. 75-79.

20. Bradbury, E. M., P. D. Cary, G. E. Chapman, C. Crane-Robinson, S. E. Danby, H. W. E. Rattle, M. Bublika, J. Palav, and F. J. Aviles, *Studies on the Role and Mode of Operation of the Very-Lysine-Rich Histone H^1 (F^1) in Eukaryote Chromatin. The Conformation of Histone H*, Eur. J. Biochem., Vol. 52, 1975 : pp. 605.

21. Lee, A. G., N. J. M. Birdsal and J. C. Metcalfe, *Measurement of fast lateral diffusion of lipids in vesicles and in biological membranes by ^{1}H nuclear magnetic resonance*, Biochem., Vol. 12, 1974 : pp. 1650-1659.

22. Chapman, B. E., S. S. Danyluk and K. A. McLuchlem, *A Model for Collagen Hydration,* Proc. Roy. Soc. London, B. Vol. 178, 1971 : pp. 465.

23. Kurosu, H. and T. Yamanobe, *Synthetic macromolecules, In : Nuclear magnetic resonance, edited by Webb, G. A.*, The Royal Society of Chemistry, Cambridge, U. K., Vol. 37, 2008 : pp. 293-326,

24. Prior, M. J. W., *NMR in living systems, In : Nuclear magnetic resonance, edited by Webb, G. A.*, The Royal Society of Chemistry, Cambridge, U. K.. Vol. 37, 2008 : pp. 327-356,

25. Jardetzky, O., *Determination of macromolecular structure and dynamics by NMR, In : NMR in the Life Sciences, Edited by Bradbury, E. M. and Nicolini, C.*, Plenum Press, New York., 1986 : pp.49-72.

26. Housnell, E., *NMR of carbohydrates, lipids and membranes, In : Nuclear Magnetic Resonance, Edited by Webb, G. S.,* The Royal Society of Chemistry, Cambridge, U. K.. Vol. 37, 2008 : pp. 274-292,

27. Simpson, P. J., *NMR of proteins and nucleic acids, In : Nuclear Magnetic Resonance, Edited by Webb, G. S.*, The Royal Society of Chemistry, Cambridge, U. K.,Vol. 37, 2008 : pp. 257-273,

28. Consonni, R. and L. R. Cagliani, *Nuclear magnetic resonance and chemometrics to access geographical origin and quality of traditional food products, In : Advances in Food and Nutritional Research*,Vol. 59, 2010 : pp. 87-164.

29. Adan, A., D. Kilian and J. G. Warren, *Applications of natural abundance carbon-13 NMR to studies of proteins and glycoproteins, In : NMR and Biochemistry, Edited by Opella, S. J. and Lu, P.,* Marcel Dekker, Inc., New York and Basel, 1979 : pp. 31-50.

30. Talebpour, Z., H. R. Bijanzedeh, S. Haghoo and M. Shamsipir, *^{1}H NMR methods for simultaneous identification and determination of caffeine and theophylline in human serum and pharmaceutical preparations*, Anal. Chem. Acta, Vol.506, 2004 : pp.97-104.

31. Wishrat, D., *NMR spectroscopy and protein structure determination. Application to drug discovery and development,* Current Pharm. Biotech.,Vol. 6, 2005 : pp. 105-120.

32. Alaxander, L., D. R. Brain, H. Kent and W. Wills, *Efficacy of proton magnetic resonance spectroscopy in neurological diagnosis and neurotherapeutic decision making.* Neuro Rx, Vol. 2, No.2, 2005 : pp. 197-214.

33. Engelhardt, E., D. M. Moreira, J. Lake and J. Cavalcanti, *Alzheimer's disease and proton magnetic resonance spectroscopy of limbic regions : a suggestion of a clinical–spectroscopic staging.* Arq. Neuropsiquiatr, Vol. 63, No. 2A, 2005 : pp. 195-200.

34. Soher, B.J., P. M. Doraiswamy and H. C. Charles, *A review of ^1H NMR spectroscopy findings in Alzheimer's disease.* Neuroimaging . Clin. N. Am.,Vol. 15, No. 4, 2005 : pp. 847-852.

35. Rhinehart, D. L., L. A. Cox and B. W. Long, *NMR spectroscopy of Alzheimer's disease. Radiol.Technol.*,Vol. 70, No. 1, 1988 : pp. 23-28.

36. Westman, E., L. O. Wahlund, C. Foy, M. Poppe, A. Cooper, D. Murphy, C. Spenger, S. Lovestone and A. Simons, *Magnetic resonance imaging and magnetic resonance spectroscopy for detection of early Alzheimer's disease.* J. Alzheimer's Dis., Vol. 26, No. Suppl 3, 2011 : pp. 307-319.

37. Azevedo, D., M. Tatsch, S. R. Hototian, M. C. Bazzarella, C. C. Castro and C. M. Bottino, *Proton spectroscopy in Alzheimer's disease and cognitive impairment no dementia : a community based study. Dement.* Geriatr. Cogn. Disord., Vol. 26, No. 5, 2008 : pp. 491-500.

38. Frederick, B.D., A. Satin, L. L. Wald, J. Hennen, N. Bodick and P. F. Renshaw, *Brain proton magnetic resonance spectroscopy in Alzheimer's disease : changes after treatment with xanomeline.* Am. J. Geriatr. Psych, Vol. 10, No. 1, 2002 : pp.81-88.

39. Jonathan, G. R. and K. Kejal, *Magnetic resonance spectroscopy in Alzheimer's disease*. Neuropsychiatr. Dis. Treat, Vol. 9, 2013 : pp. 687-696.

40. Colla, M., G. Ende, M. Bohrer, M. Deuschle, G. Kronenberg, F. Henn and I. Heuser, *NMR spectroscopy in Alzheimer's disease : gender differences in probabilistic learning capacity.* Neurobiol. Aging , Vol. 24, No. 4, 2003 : pp. 545-552.

41. Chen, J. G., H. C. Charles, D. P. Barboriak and P. M. Doraiswamy, *Magnetic resonance spectroscopy in Alzheimer's disease : focus on N-acetylasparatate.* Acta.Neurol.Scand Suppl.,Vol.176, 2000 : pp.20-26.

42. Kantarci, K., *^1H magnetic resonance spectroscopy in dementia*. Br. J. Radial.,Vol. 80, No.2, 2007 : pp. S146-152.

43. Doraiswamy, P. M., H. C. Cahrles, K. Ranga ramkrishna, *Prediction of cognitive decline in early Alzheimer's disease.* The Lancet, Vol. 352, No. 9141, 1998 : pp.1678.

44. Antuono, P. G., L. J. Jennifer, W. Yonker and Jiang, L. Shi, *Decreased glutamate + glutamine in Alzheimer's disease detected in vivo with ^1H MRS at 0.5 T .Neurology*, Vol. 56, No. 6, 2001: pp. 737-742.

45. Chantal, S., M. Labelle, R.W. Bouchard, C. M. Braun and Y. Boulanger, *Correlation of regional proton magnetic resonance spectroscopic metabolic changes with cognitive deficts in mild Alzheimer's disease*. Arch.Neurol, Vol.59,No.6, 2002 : pp. 955-962.

46. Kantarci, K., R. C. Peterson, B. F. Boeve, D. S. Kncpman, D. F. Tang-Wai, P. C. Ỏ Brain, S. D. Weigand, S. D. Edland, G. E. Smith, R. J. Ivnik, T. J. Ferman, E. G. Tangalos, and C. R. Jack Jr., *^1H NMR spectroscopy in common dementias*.Neurology , Vol. 63, No. 8, 2004 : pp. 1393-1398.

47. Huang, W., G. E. Alaxander, L. Chang, H. U. Shetty, J. S. Krasuski, S. I. Rapoport, and M. B., Schapiro, *Brain metabolite concentration and dementia severity in Alzheimer's disease.* Neurology, Vol. 57, No.4, pp. 2001 : 626-632.

48. Shiino, A., M. Matsuda, S. Morikawa, T. Inbhushi, I. Akiguchi and J. Handa, *Proton magnetic resonance spectroscopy with dementia*. Surg. Neurology, Vol. 39, No. 2, 1993 : pp. 143-147.

49. Shonk, T. K., R. A. Moats, P. Gifford, T. Michaelis, J. C. Mandigo, J. Izumi and B. D. Ross, *Probable Alzheimer's disease: diagnosis with proton MR spectroscopy.,* Radiology, Vol. 195, No. 1, 1995 : pp. 65-72.

50. Alexandra, J. S., Alexandra, K. B., Elizabeth, A.W., Paul, M.S., Saaeha, R. and Stephan, P. Y., *NMR based metabolonic analysis of cerebrospinal fluid and serum in neurological diseases –a diagnostic tool? NMR. Bio*. Med., Vol.23, No. 2, 2010 : pp. 123-1321.

51. Tukiainen, T., Tunkkynen , T., Mȧkinen ,V. P., Jylȧnki, P., Kangas, A., Hokkanen, J., Vehtari, A, Grőhn, O., Hallikainen, M., Soininen, H., Kivipelto, M., Groop, P. H., Kaski, K., Laatikainen, R., Soininen, P. Pirttila, T. and Ala-Korpela, M., *A multi–maetabolite analysis of serum by ^{1}H NMR spectroscopy ; Early systemic signs of Alzheimer's disease*, Biochem. Biophys. Res. Commmun., Vol. 375, 2008 : pp. 356-361.

52. Ghauri, F. Y. K., Nicholson, J. K., Sweatman, B. C., Wood, J., Beddell, C. R., Lindon, J. C. and Cairns, N. J., *NMR spectroscopy of human post mortem cerebrospinal fluid : Distinction of Alzheimer's disease from control using pattern recognition and statistics.* NMR. Biomed , Vol. 6, No.2, 1993 : pp.163-167.

53. Bell, J. D., Brown, J. C. C. and Sadlev, P. J., *NMRstudies of body fluids.* NMR. Biomed, Vol. 2, 1989 : pp. 246-256.

54. Hudson, L. and Hay, F. C., *Practical immunology,* 2nd edition, Black Well Scientific Publication, Oxford, London, Edinburg, Boston, Melbourne, 1980 : pp. 22

55. Mandel, M., *Proton Magnetic Resonance Spectra of some Proteins Ribonuclease*, Oxidized Ribonuclease Lysozyme and Cytochrome C", J. Biochemistry, Vol. 240, 4, 1965 : pp. 1586-1592.

56. Vitolis, C. and Weljie, A., *Identifying and qualifying metabolites in blood serum and plasma", Chenomx App Note,* http://www.chenomx.com. 2006 : pp.

57. Burton, D. R., *Paramagnetic ions as relaxation probes in biological systems", In : ESR and NMR of paramagnetic species in biological and related systems, Bertini I. and Drago R. S. (eds.),* Reidel, Dordrecht, Holland, 1980 : pp. 151.

58. Mayer, M., *The complement system", In : "Immunology, Readings from Scientific American", Burnet, F. M. (ed.),* Freeman, W. H. & Co., San Francisco, 1976 : pp. 143-155.

59. Huber, H., Deisenhofer, J., Colman, P. M., Matsushima, M. and Palm, W., *Crystallographic structure of an IgG molecule and Fc fragment", Nature*, Vol.264, 1976 : pp. 415-420.

60. Boyd, J., Easterbrook-Smith, S. B., Zavodsky, P., Mountford-Wright, C. and Dwek, R. A., *Mobility and symmetry in the Fc and pFc' fragments as probed by ^{1}H NMR", Mol. Immunol.*, Vol. 16, No. 11, 1979 : pp. 851-8.

61. Cohen, J. S., L. J. Hughes and J. B. Wooten, *Observations of amino acid side chain in protein by NMR methods, In : Magnetic Resonance in Biology, edited by Cohen, J. S.,* 3, John Wiley & Sons, New York, Singapore, 1983 : pp. 130-247.

62. Kumar, A., G. Wagner, R. R. Ernst and K. Wuthrich, *Build up roles of the nuclear overhouse effects measured by two-dimensional proton magnetic resonance spectroscopy : Implications for studies of protein information",* J. Am. Chem. Soc., Vol.103,No. 13, 1981 : pp. 3654-3658.

63. Nagayama, K. and K. Withruch, *Systematic application of two-dimensional nuclear magnetic resonance techniques for studies of protein 1. combined use of spin-echo-correlated spectroscopy and J-resolved spectroscopy for the identification of complete spin systems of non-labile protons in amino acid residues",* Eur. J. Biochem., Vol.114, 1981 : pp. 365-374

64. Wagner, G., A. Kumar and K. Wuthrich, *Systematic application of two-dimensional ^{1}H nuclear magnetic resonance techniques for studies of protein 2. Combined use of correlated spectroscopy and nuclear*

overhouse spectroscopy for sequential assignment of backbone resonance and elucidation of polypeptide secondary structures", Eur. J. Biochem , Vol. 114, 1981 : pp. 375 .

65.   Glick, R. E., D. F. Kates, and S. J. Ehrenson, *Applicability of the macroscopic magnetic susceptibility model to solvent effects in nuclear magnetic resonance, J. Chem. Phys.*, Vol. 31, 1959 : pp. 567 .

66.   Moore, R. and R. J. P. Williams, *Nuclear magnetic resonance studies of eukaryotic cytochrome C assignment of resonance of aromatic amino acids,* Eur. J. Biochem., Vol.103, 1980 : pp. 493-502.

67.   Spera, S. and A. Bax, *Empirical correlation between protein backbone conformation and C alpha and C beta 13 nuclear magnetic resonance chemical shifts,* J. Am. Chem. Soc., Vol.113, 1991 : pp. 5490-5492.

68.   Kuszewski, J., Q., A. M. Gronenborn, G. M. Clore, *The impact of direct refinement against ^{13}C and ^{13}C chemical shifts on protein structure determination by NMR*, J. Mag. Res. B., Vol.106 ,No.1, 1995 : pp. 92-96.

69.   Withrat, D. S. and B. D. Sykes, *The ^{13}C chemical shift index : a simple method for the identification of protein secondary structure using ^{13}C chemical shift data, J. Biomol. NMR*, Vol. 4, 1994 : pp. 171-180.

70.   Wang, Y. J. and O. Jardetzky, *Probability based protein secondary structure identification using combined NMR chemical shift data,* Protein Sci., Vol.11, 2002 : pp. 852-861.

71.   Cornilescu, G., F. Delaglic and A. Bax, *Protein backbone angle restraints from searching a data base for chemical shift in a sequence homology,* J. Biomol. NMR,Vol. 13, 1994 : pp. 289-302.

72.   Cavalli, A., X. Salvatella, C. M. Dobson, and M. Vendruscola, *Protein structure determination from NMR chemical shifts,* Proc. Natl. Acad. Sci., USA, 104, 2007 : pp. 9615-9620 .

73.   Shen, Y., O. Lange, F. Delaglio, P. Rossi, J. M. Aramini, G. H. Liu, A. Eletsky, Y. B. Wu, K. K. Singarapu, A. Lemak, A. Ignatchenko, C. H. Arrowsmith, T. Szperski, G. T. Montelione, D. Baker and A. Bax, *Consistent blind protein structure generation from NMR chemical shift data*, Proc. Natl. Acad. Sci., USA, Vol.105, 2008 : pp. 4685-4690.

74.   Withrat, D. S., A. D. Arndt, M. Berjanskii, P. Tang, J. Zhou and G. Lin, *CS$_2$3D: awes server for rapid protein structure generation using NMR chemical shifts and sequence data,* Nucleic Acids Res., Vol.36, 2008 : pp. W496-W502 .

75.   Montalvao, R. W., A. Cavalli, X. Aalvatella, T. L. Blundell and M. Vendruscok, *Structure determination of protein and protein complexes using NMR chemical shifts : case of an endonuclease colicin and immunity protein complex*, J. Am. Chem. Soc., Vol.130, No. 4, 2008 : pp. 15990-15996.

76.   Dominguez, C., D. Boelens and A. M. J. J. Bonvin, *A protein and protein docking approach and biochemical or biophysical information*, J. Am. Soc., Vol. 125, No.7, 2003 : pp. 1731-1737.

77.   Satoshi, E. and Y. Arata, *Proton nuclear magnetic resonance study of human immunoglobulin G1 and their proteolytic fragments : Structure of the hinge region and effects of a hinge region deletion on internal flexibility*, Biochemistry, Vol. 24, No.6 , 1985 : pp. 1561-1568.

78.   Koichi, K., C. S. Fridman, W. Yamada, K. Kabayashi, S. Uchiyama, H. H. Kim, J. Fenokizono, A. Galinha, Y. Kobayashi, W. H. Fridman, Y. Arata, and I. Shimada, *Structural basis of the interaction between IgG and fcy receptors,* J. Mol. Biol., Vol.295, No.2, 2000 : pp. 213-224.

79.   Brab, A. W. and J. H. Prestegard, *NMR analysis demonstrates immunoglobulin GN-glycans are accessible and* dynamic *nature,* Chemical Biol., 7, 2011 : pp. 147-153.

80.   Nicholson, L. K., L. E. Kay, D. M. Boldisseri, J. Arange, P. E. Young, A. Bax, D. A. Torchia, *Dynamics of methyl group in proteins as studied by proton detected 13C NMR spectroscopy : application to the leucine residues of staphylococcal nuclease,* Biochemistry, Vol. 31, 1992 : pp. 5253-5263.

81.   Szilagye, L. and O. Jardetzky, *Alpha proton chemical shifts and secondary structure in proteins,* J. Magn. Reson.,Vol. 83, 1989 : pp. 441.

82.   Pastore, A., U. Saudek, *The relationship between chemical shift and secondary structure in proteins*, J. Magn. Reson.,Vol. 90, 1990 : pp. 165-176.

83.   Oldfield, E., *Chemical shifts and three dimensional protein NMR structures*, J. Biomol., Vol.5, 1995 : pp. 217-225.

84.   Jardetzky, O. and C. D. Jardetzky, *Proton magnetic resonance spectra of amino acids, J. Biol. Chem.* 233, 1958 : pp. 383.

85 .   Chandra, R.K., *Trace Elements and Immunity : A Synopsis of current knowledge*. The United Nations University// internet news pp.1-3

86.   Tourtellotte, W., *On cerebrospinal fluid immunoglobulin – G (IgG) quotients in multiple sclerosis and other disease A review and a new formula to estimate the amount of IgG synthesized per day by the central nervous system*. J .Neurol .Sci, Vol.10 and No. 279, 1970 : pp.304